Age-Optimal Network Coding HARQ Transmission Scheme for Dual-Hop Satellite-Integrated Internet

Jian Jiao, *Member, IEEE*, Shiqi Liu, Jing Ding, Jianhao Huang, Shaohua Wu, *Member, IEEE*, Rongxing Lu, *Fellow, IEEE*, and Qinyu Zhang, *Senior Member, IEEE*

***Abstract*—In the upcoming satellite-integrated Internet, a noted limitation is the non-trivial propagation latency due to the long distances. To support the emergent timeliness applications, information must be transmitted within a short end-to-end latency. Hence, the traditional hybrid automatic repeat request (HARQ) strategies with frequent feedbacks do not fit anymore, because the reliable transmission needs retransmission of the lost packets, which inevitably leads to the low efficiency in the satellite-integrated Internet. In this paper, we propose an age-optimal network code HARQ (NC-HARQ) transmission scheme with the metric of information timeliness, i.e., age of information (AoI) to realize limited/no feedback dual-hop reliable transmission in the satellite-integrated Internet. We derive the closed-form expression for the average and peak AoI of the proposed dual-hop age-optimal NC-HARQ transmission scheme, and also the expression for the benchmark schemes through establishing a finite-state Markov chain. Then, by taking account of the time-varying channel and the characteristics of random update of data file, two dynamic forward transmission strategies are further designed. Simulation results illustrate that our dual-hop age-optimal NC-HARQ transmission scheme can achieve lower average and peak AoI in comparison with several state-of-the-art HARQ schemes.**

***Index Terms*—Satellite-integrated Internet, timeliness, age of information, network coding, HARQ.**

I. Introduction

With the commercial applications of fifth generation (5 G) mobile communications, the satellite-integrated Internet has become an important research direction in the beyond 5 G (B5G) and even in the future sixth generation (6 G) [1], [2]. Since the end-to-end satellite communication is faster than the terrestrial fiber optic networks under the distance larger than 3000 kilometers [3], the upcoming satellite-integrated Internet has the potential to well support numerous emerging timeliness applications in the global coverage [4], such as intelligent traffic, smart grid, voyage navigation and disaster relief [5]. Consider that the information freshness is a stringent requirement for the above mentioned timeliness services in the satellite-integrated Internet [6], to evaluate the freshness of information, a timeliness metric named age of information (AoI) is introduced in this paper. Note that AoI was originally introduced in [7], which is defined as the time elapsed since the timestamp of the most recently received update [8].

Nevertheless, the long distance and complicated environment between satellite and terrestrial devices and base station would lead to high bit error rate (BER) and even outage. Thus, the bit-level forward error correction (FEC) approaching the Shannon limit still can not guarantee the reliable transmission of data packets [9]. Therefore, at the link layer, the failure decoded packet is treated as lost and needs retransmission. However, the conventional reliable retransmission schemes, such as hybrid automatic repeat request (HARQ), would lead inefficient for the lost data packets recovery in the satellite-integrated Internet, since additional retransmission rounds significantly increase the end-to-end delay due to the non-trivial propagation latency and frequent link disruptions.

To tackle this issue, the consultative committee for space data systems (CCSDS) released the long erasure code (LEC) specification [10], where a packet-level LEC is proposed at the link layer to help mitigating the packet loss by the physical layer bit-level FEC. Thus, the receiver can utilize the packet-level LEC to help recovering the failure decoded or congestion lost packets in physical layer, which could approach a required file error rate (FER) if receives sufficient LEC packets. Therefore, we introduce a network coded (NC) HARQ scheme as the LEC scheme for the reliable transmission [11] in the multi-hop satellite-integrated Internet transmission scenario to reduce FER and enhance the timeliness, and focus on the design of a dual-hop age-optimal NC-HARQ transmission scheme to lower the AoI and ensure the reliability.

A. Related Works and Motivation

Since the propagation latency is non-trivial in the satellite-integrated Internet, the traditional end-to-end transmission delay

Manuscript received 11 February 2022; revised 8 June 2022; accepted 20 June 2022. Date of publication 24 June 2022; date of current version 17 October 2022. This work was supported in part by the National Natural Sciences Foundation of China (NSFC) under Grants 62071141, 61871147, 61831008, and 62027802, in part by the Natural Science Foundation of Guangdong Province under Grant 2020A1515010505, in part by Guangdong Science and Technology Planning Project under Grant 2018B030322004, in part by the Shenzhen Science and Technology Program under Grants ZDSYS20210623091808025 and GXWD20201230155427003-20200822165138001, and in part by the Major Key Project of PCL under Grant PCL2021A03-1. The review of this article was coordinated by Prof. Daniele Tarchi. *(Corresponding author: Qinyu Zhang.)*

Jian Jiao, Shiqi Liu, Jing Ding, Jianhao Huang, Shaohua Wu, and Qinyu Zhang are with the Communication Engineering Research Centre, Harbin Institute of Technology (Shenzhen), Shenzhen 518055, China, and also with the Peng Cheng Laboratory, Shenzhen 518055, China (e-mail: j.jiao.hitsz@foxmail.com; 19s152087@stu.hit.edu.cn; 20s152068@stu.hit.edu.cn; 180210220@stu.hit.edu.cn; hitwush@hit.edu.cn; zqy@hit.edu.cn).

Rongxing Lu is with the Faculty of Computer Science, University of New Brunswick, Fredericton, NB E3B 5A3, Canada (e-mail: rlu1@unb.ca).

Digital Object Identifier 10.1109/TVT.2022.3186034

cannot characterize the timeliness of data services, and the concept of age of information (AoI) is introduced [12]. AoI is defined as the amount of time elapsed since the generation of the last received update, and average AoI is the average age over all time. The method of adding AoI to the tandem queue model has firstly appeared in [13], which considers a single server queue in the terrestrial transmission. The combination of AoI and single hop end-to-end transmission with a computation queue is analyzed in [14], [15], where the average AoI and peak AoI in four different tandem queue models are analyzed. The authors in [16] analyze the average AoI in a tandem queue with two nodes under the condition of zero-waiting. [17] has analyzed the average AoI in the multi-hop satellite communication scenario without considering the transmission protocol. Moreover, HARQ is commonly regarded as a reliable transmission scheme in terrestrial network to ensure/tradeoff the reliability and efficiency [18]. The high reliability of HARQ is achieved by using successive retransmissions and feedbacks to combat the bad channel conditions [19]. In [20], [21], the performance of both incremental redundancy (IR)-HARQ and chase combining (CC)-HARQ with finite blocklength codes over a Rayleigh block fading channel are analyzed. However, the above mentioned HARQ protocols are inefficient due to their acknowledgement/negative acknowledgement (ACK/NACK) feedbacks, and the lost packet retransmissions would lead to severely degrade the timeliness as the propagation latency is non-trivial in the satellite-integrated Internet [22], [23]. In [24], some retransmissions and feedbacks are omitted in the HARQ process to accelerate the transmission. [25] sets the maximum retransmission rounds as a dynamic value to improve the transmission quality. Note that the CCSDS releases the Licklider Transmission Protocol (LTP) [26], which is adopting the asynchronous NAK feedback HARQ retransmission to significantly reduce the feedback and retransmission rounds.

Note that most of the related HARQ schemes focus on the file delivery delay and throughput without considering the AoI performance in the satellite-integrated Internet. The combination of AoI and end-to-end transmission scheme has been analyzed in [27], [28]. Specifically, the freshness of K status packets update through the erasure channels with error-free feedback is investigated in [27], and the AoI of K status packets is modeled without designing a HARQ transmission scheme. However, there is still lack of work on the AoI performance and joint design of the dual-hop HARQ transmission scheme. In detail, we should transmit sufficient NC packets to guarantee the FER and lower the AoI, while excessive NC packets would lead to the increasing of delay and wasting of energy. Therefore, we propose an age-optimal NC-HARQ transmission scheme for dual-hop satellite-integrated Internet in this paper, and focus on the tradeoff among the AoI, delay and FER to design the corresponding relay modes.

B. Contributions

The novelties and contributions of this paper can be summarized as follows:

- We propose an *age-optimal NC-HARQ* transmission scheme for the dual-hop satellite-integrated Internet communication scenario to minimum the average/peak AoI, where the sender and relay satellite utilize the NC to perform LEC to encode original packets. Then, the relay satellite and ground station can recover the lost original packets via the NC packets to avoid retransmission. We derive the BER expression of shadowed-Rician fading channel to derive the FER in our system, which provides a theoretical fundament to estimate the appropriate number of NC packets to guarantee lower AoI and end-to-end delay.
- We further propose two relay modes in our *age-optimal NC-HARQ* transmission scheme, named NC-HARQ with no retransmission (NCnr-HARQ) mode and NC-HARQ with one-time retransmission (NCor-HARQ) mode, respectively. In detail, if the satellite fails to decode the file then the file is discarded in the NCnr-HARQ mode. On the other hand, in the NCor-HARQ mode, if the satellite fails to decode, then it feeds back the instant CSI and the ground devices can perform one-time retransmission according to the feedback CSI. Then, to yield the insight into the performance of our *age-optimal NC-HARQ* transmission scheme, we derive the closed-form expressions of the average/peak AoI by using a discrete two-state Markov chain in the first-hop transmission, and a four-state Markov chain in the second-hop transmission. In addition, we derive the closed-form expressions of the end-to-end expected delay and throughput.
- We verify the accuracy of theoretical analysis through various Monte Carlo simulations, and further evaluate the average/peak AoI, end-to-end expected delay and throughput, and compare with other state-of-the-art transmission schemes including Fast HARQ [24] and dynamic-HARQ (D-HARQ) [25]. Simulation results show that our *age-optimal NC-HARQ* owns better performance than the Fast HARQ and D-HARQ schemes. Specifically, the NCnr-HARQ mode can lower the long-term transmission delay and increase the throughput. The NCor-HARQ mode can decrease the BER and achieve the lowest average/peak AoI. Moreover, the NCor-HARQ mode can guarantee the reliable transmission by utilizing one-time retransmission, which also illustrates that the retransmission can be limited in one round in our *age-optimal NC-HARQ* transmission scheme.

C. Outline

The rest of the paper is organized as follows. In Section II, we introduce the equivalent tandem queue, the channel model and the age-optimal NC-HARQ transmission scheme. In Section III, we establish the AoI evolution models and derive the closed-form expressions of average AoI and peak AoI, then we derive the end-to-end delay and throughput of the age-optimal NC-HARQ transmission scheme for both the single-hop and dual-hop scenarios, we further evaluate the end-to-end delay and throughput of the Fast HARQ and D-HARQ schemes.

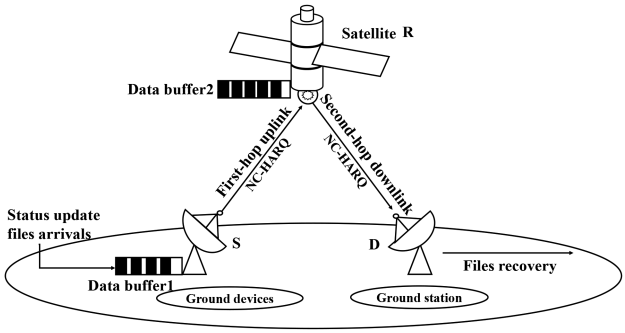

Fig. 1. Dual-hop satellite-integrated Internet transmission, where the satellite receives data from ground devices and then relays to the ground station.

In Section IV, we present the simulation results. Finally, we conclude the paper in Section V.

II. System Model

We consider a dual-hop satellite-integrated Internet transmission scheme as depicted in Fig. 1. A relay satellite R covers a wide remote area on Earth and receives data generated from ground device S in line of sight (LoS) link, and the age-critical data packets from S are relayed to R and then forwarded to a ground station D as soon as possible. The channel from S to R and R to D are both modeled as shadowed-Rician fading channel.

A. Dual-Hop Tandem Queue Model

We model this dual-hop transmission as a tandem queue consisting of two transmission queues as shown in Fig. 1, where both transmission queues are in the form of $M/M/1$. The arriving files to the first queue in S follow the Poisson process with arrival rate λ_1, the end-to-end delay from S to R follows an exponential distribution with random variable μ_1, and the corresponding waiting time is w_1. Similarly, the arriving files to the second queue in R is with the exponential inter-departure times $1/\lambda_2$, which is determined by λ_1, μ_1 and w_1. The corresponding end-to-end delay from R to D also follows the exponential distribution with random variable μ_2, and the corresponding waiting time is w_2. Note that μ_1 and μ_2 depend on the specific channel state in the dual-hop satellite-integrated Internet transmission scenario. Without loss of generality, we assume that all the arriving files consist of the same amount χ and the same length of packets, and S and R handle one file at a time.

In our equivalent queue model, S and R are equipped with single buffer with infinite capacity, which is ruled by Last Come First Served (LCFS) policy with discarding to achieve the highest freshness. Specifically, both queues have two states named Idle (Id) and Busy (B), thus, if a coming file arrives at the queue finds that no file is being served, i.e., S or R is in Id state, then the transmission process starts right away; Otherwise S or R is in B state, and it waits in the buffer till the current file transmission is finished. Note that S and R adopt the LCFS policy, if several files arrive at the queue when the nodes are in B, only the latest file in the buffer is to be served and other buffered files are discarded directly.

B. Channel Model

The channel of the satellite-integrated Internet can be modeled as the widely used shadowed-Rician (SR) fading distribution [29], and the CSI remains the same in the duration of a file transmission period, and randomly changes at the beginning of the next file transmission. Thus, the probability density function (PDF) of SR fading distribution is given by [30]

$$f(x) = \frac{1}{2b_0\gamma}\left(\frac{2b_0 m}{2b_0 m+\Omega}\right)^m \exp\left(-\frac{x}{2b_0\gamma}\right) \cdot {}_1F_1\left(m, 1, \frac{1}{2b_0\gamma}\left(\frac{\Omega}{2b_0 m+\Omega}\right)x\right), \quad (1)$$

where ${}_1F_1(.,.,.)$ is the confluent hypergeometric function, γ denotes the average value of signal noise ratio (SNR), Ω is the average power of LoS component, $2b_0$ is the average power of the multipath component, and $m(m \geq 0)$ is the parameter of channel fading severity.

The derivation of BER in SR fading channel as follows:

$$P_e = \sum_{k=0}^{m-1} \alpha\theta_k \sum_{j=1}^{\max(M/4,1)} \frac{1}{\xi_M} \cdot \left(\frac{1}{\eta^{k+1}} - \frac{1}{\sqrt{2\pi}}\sum_{i=0}^{k}\frac{1}{i!}\frac{1}{2^{i-v}b_j^{2i}\eta^{k-i+1}\left(1+\eta/b_j^2\right)^v}\Gamma(v)\right) \quad (2)$$

where $\alpha = \frac{1}{2b_0\gamma}(\frac{2b_0 m}{2b_0 m+\Omega})^m$, $\eta = \frac{m}{(2b_0 m+\Omega)\gamma}$, $v = \frac{2i+1}{2}$, $\xi_M = \max(\log_2 M, 2)$, $b_k = \sin\frac{(2k-1)\pi}{M}$, $\theta_k = \frac{(-1)^k(1-m)_k}{k!}(\frac{1}{2b_0\gamma}\frac{\Omega}{2b_0 m+\Omega})^k$ and Γ is the Gamma function. The detailed derivation process of the BER is given in Appendix A.

Due to the fact that SR fading channel is volatile, we can find that each average SNR γ owns a good instant SNR r_g and a bad instant SNR r_b according to (1). Then, we can set an appropriate SNR threshold r_t for different γ in SR fading channel to divide two channel states, i.e., $good$ and bad states. In detail, if the instant SNR falls into the interval $[r_t, r_g]$, then the current channel condition is in $good$ state; Otherwise, it is in bad state. Moreover, we can convert r_g, r_t and r_b to P_{eg}, P_{et} and P_{eb} based on (1) and (2). Specifically, the stationary probabilities of $good$ and bad states are derived as $P = [\Pr(g) \quad \Pr(b)]$, which can be expressed as follows,

$$\Pr(\mathrm{g}) = \int_{r_t}^{r_g} f(r)dr = \sum_{k=0}^{m-1}\alpha\theta_k e^{-\eta r_t}\sum_{i=0}^{n}\frac{1}{i!}\frac{r_t^k}{\eta^{k-i+1}}, \quad (3)$$

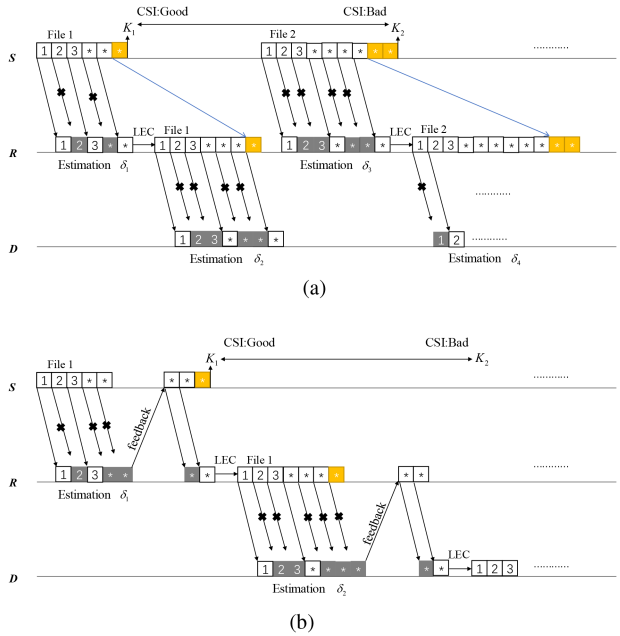

Fig. 2. A dual-hop illustration of our age-optimal NC-HARQ transmission scheme. (a) NCnr-HARQ relay mode. (b) NCor-HARQ relay mode.

and

$$\Pr(b) = \int_{r_b}^{r_t} f(r)dr = 1 - \sum_{k=0}^{m-1} \alpha\theta_k e^{-\eta r_t} \sum_{i=0}^{n} \frac{1}{i!} \frac{r_t^k}{\eta^{k-i+1}}. \quad (4)$$

Therefore, the time-varying SR fading channel can be modeled as a two-state Gilbert-Elliott (GE) channel based on the required P_{et} and the transition probability matrix is as follows:

$$\mathbf{G} = \begin{bmatrix} \Pr(g \mid g) & \Pr(b \mid g) \\ \Pr(g \mid b) & \Pr(b \mid b) \end{bmatrix} = \begin{bmatrix} \sigma_1 & 1-\sigma_1 \\ \sigma_0 & 1-\sigma_0 \end{bmatrix}, \quad (5)$$

where $\Pr(g \mid g) = \sigma_1$ is the probability that the SR fading channel stays in *good* state, $\Pr(g \mid b) = \sigma_0$ is the probability that the channel state changes from *bad* to *good* ($1 > \sigma_1 > \sigma_0 > 0$).

C. Dual-Hop Age-Optimal NC-HARQ Transmission Scheme

The proposed age-optimal NC-HARQ transmission scheme for dual-hop satellite-integrated Internet is depicted in Fig. 2. The basic idea of age-optimal NC-HARQ transmission scheme is to utilize appropriate number of NC packets to recover the erasure packets at the receiver to reduce feedback and retransmission. Moreover, our age-optimal NC-HARQ transmission scheme can be further extended to two relay modes to deal with different AoI requirement, named NC-HARQ with no retransmission (NCnr-HARQ) mode as shown in Fig. 2(a), and NC-HARQ with one-time retransmission (NCor-HARQ) mode as shown in Fig. 2(b). The detail of NCnr-HARQ and NCor-HARQ relay modes are summarized as follows:

Step 1: The first-hop transmission from S to R. Before the beginning of the transmission, S can get the delayed CSI through belief probability p, e.g., if the previous state is *good*, then R feedbacks one bit as 1, otherwise is 0. Thus, there are two actions for S that can be chosen at the beginning of each file transmission, which can be described in detail as follows.

Action A (Betting aggressively): When S firmly believes that the channel has a high chance in *good* state, S transmits a high number R_h of data bits.

Action C (Betting conservatively): When S believes that the channel is in *bad* state, then it transmits a low number R_l of data bits.

Then, we have the following optimal transmission policy [32].

Theorem 1: If $R_l/R_h < \sigma_0$, the optimal transmission action is A; If $R_l/R_h > \sigma_1$, the optimal transmission action is C; Moreover, if $\sigma_0 \leq R_l/R_h < \sigma_1$, when the delayed feedback CSI is 1, the optimal transmission action is A, and when the delayed feedback CSI is 0, the optimal action is C.

Therefore, in the NCnr-HARQ relay mode, S determines the number of NC packets to guarantee the reliable transmission via the delayed feedback of CSI in the last transmission according to **Theorem 1**. If it takes action A, then $R_h = (1 - P_{et})/\chi$, which means that S encodes χ original packets to $\delta_1 = \chi/(1 - P_{et})$ NC packets and sends to R, and the upper bound of NC packets is denoted as K. If it takes action C, then $R_l = (1 - P_{eb})/\chi$, which means that S encodes χ original packets to $\delta_1 = \chi/(1 - P_{eb})$ NC packets. Then, R does not begin the decoding or send feedback signals until finds that δ_1 NC packets transmission are finished, which can be known from the meta-data in the packets [26]. Then, R combines the successfully received NC packets to recover the χ original packets. If it succeeds, R forwards this file to the second-hop transmission as shown in the following Step 2. Otherwise, the file is discarded to lower the long-term transmission delay if R fails to decode the file.

As for the NCor-HARQ relay mode, similarly, S firstly makes the estimation through the transition probability in (5). However, if it takes action A, then S encodes χ original packets to $\delta_1 = \chi/(1 - P_e g)$ NC packets. If it takes action C, then S encodes χ original packets to $\delta_1 = \chi/(1 - P_e t)$ NC packets and transmit to R. Then, R does not begin the decoding or send feedback signals until finds that δ_1 NC packets transmission are finished. If it succeeds, R forwards this file to the next-hop transmission as shown in the following Step 2. Otherwise, R feedbacks the instant CSI precisely in its NACK based on the total information collected yet. Then S can encode v_L NC packets ($\delta_1 + v_L = \delta_F \leq K$) according to the feedbacked CSI and perform one-time retransmission of this file. The NCor-HARQ mode can decrease the FER than the NCnr-HARQ mode, and achieve the lowest average/peak AoI.

Step 2: The second-hop transmission from R to D. In this step, R does the same channel estimation as the first-hop transmission no matter it is in NCnr-HARQ or NCor-HARQ mode. Similarly, R then performs NC to encode the received original packets to δ_2 NC packets and transmit to D. Nevertheless, the difference between the first-hop and second-hop lays in the coding upper bound. Specifically, if the file is successfully decoded with sending fewer packets than K in the first-hop transmission, then R can encode more NC packets for the second-hop. Thus, the coding upper bound at R is a dynamic value K_d, which can

be more than K. Also, during the period of δ_2 NC packets transmission, D does not send feedback signals or begin the decoding until δ_2 NC packets transmission are finished. Then, D combines all the received NC packets to decode the χ original packets, and R performs the NCnr-HARQ or NCor-HARQ mode as the same as S in Step 1.

III. Analytical Results

In this section, we first establish the AoI evolution models and derive the closed-form expressions of average AoI and peak AoI (PAoI). Then, we derive the end-to-end delay and throughput of the age-optimal NC-HARQ transmission scheme for both the single-hop and dual-hop scenarios. Further, we evaluate the end-to-end delay and throughput of the Fast HARQ and D-HARQ schemes for the later comparisons.

A. AoI Evolution Model

We exhibit the evolution of AoI in the total dual-hop, the first-hop and the second-hop under the tandem queue mentioned in Fig. 1 for a detailed analysis as shown in Fig. 3(a), (b) and (c), respectively.

As shown in Fig. 3(a), file 1, file 3 and file 5 arrive steadily at the ground device S at t_0, t_4 and t_{11}, and succeed to be decoded in R at t_2, t_6 and t_{13} and succeed to be decoded in D at t_5, t_{10} and t_{14}, respectively. File 2 owns a successful transmission in the first-hop but fails its delivery in the second-hop. File 4 is discarded due to the failed decoding in R.

The AoI of the first-hop transmission is shown in Fig. 3(b) in detail. File 1 reaches S at t_0, and then delivery to R under the age-optimal NC-HARQ transmission scheme, and R successfully decodes the file 1 at t_2. File 2 arrives S at t_1 when S is in B, and it waits for the transmission of file 1 finished at t_2, and begin its transmission at the same time, then R recovers it at t_3. File 3 comes at t_4 while S is in Id, and it immediately begins the transmission and finishes at t_6. Nevertheless, file 4 comes at t_8 while S is in Id, and it fails to be decoded in R at t_9. In the end, file 5 arrives and begins its delivery at t_{11}, and is decoded in R at t_{13}.

Then, the AoI of the second-hop transmission is shown in Fig. 3(c). R performs network encoding to file 1 and forward it at t_2, and D successfully recover it at t_5. File 2 arrives R at t_3 when R is in B, and it waits for the transmission of file 1 finished at t_5, and begin its transmission at the same time, but it fails to be decoded in D at t_7. Similarly, file 3 arrives R at t_6 when R is in B, and begin its transmission at t_7, and D successfully recover it at t_{10}. File 5 comes at t_{13} while R is in Id, and it immediately begins the second-hop transmission and finishes at t_{14}.

B. Evaluating Average AoI and Peak AoI

Let T_i^ζ and w_i^ζ denote the end-to-end delay and wait time of file i at the ζ-hop ($\zeta = 1, 2$), respectively. For example, the first-hop and second-hop end-to-end delay of file 1 is $T_1^1 = t_2 - t_0$ and $T_1^2 = t_5 - t_2$, respectively. Let T_i and W_i denote the end-to-end delay and wait time of file i in the dual-hop transmission queues, thus, $W_i = w_i^1 + w_i^2$, where w_i^1 and w_i^2 are the waiting

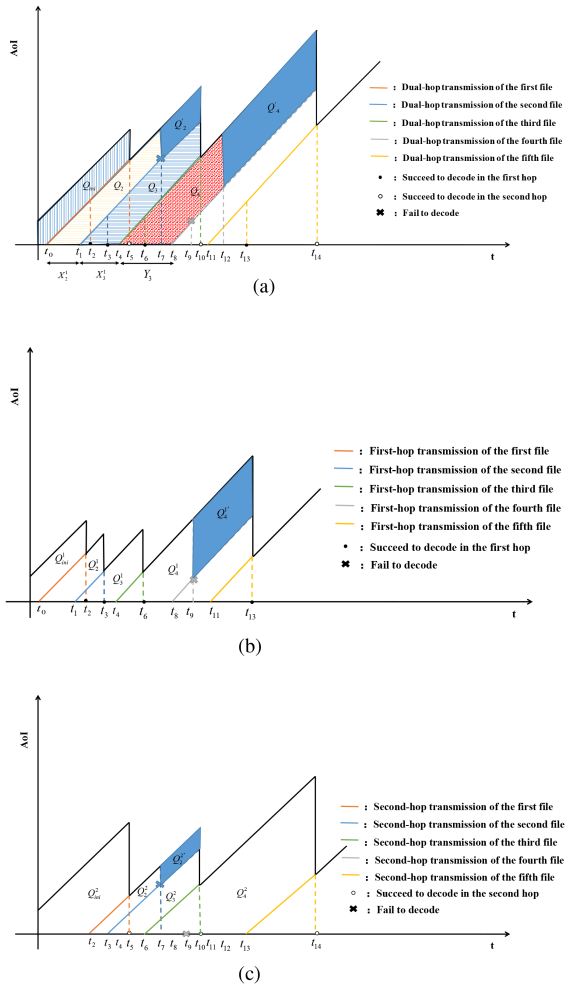

Fig. 3. The AoI evolution sample path of first-hop, second-hop, and the whole dual-hop age-optimal NC-HARQ transmission scheme with file loss and discard. (a) AoI evolution model of the dual-hop. (b) AoI evolution model of the first-hop. (c) AoI evolution model of the second-hop.

time of the first- and second-hop, respectively. We define the time interval between the files $i-1$ and i as X_i ($i \geq 2$), and X_i^ζ denotes the time interval between the files $i-1$ and i in the ζ-hop. The system time of the total two-hop transmission of file i is denoted as Y_i, where $Y_i = W_i + T_i$. Specifically, in the first-hop, we have $Y_i^1 = T_i^1 + w_i^1$, and in the second-hop is $Y_i^2 = T_i^2 + w_i^2$. Also, we define the areas under the trapezoid regions as Q_i, which is in the same order of the files arriving steadily at S. Specifically, the blue shadowed area depicted in Fig. 3(a) shows the increasing of AoI when a file is failed to decode and then discarded.

According to the definition of average AoI without considering the file lost in [17], we have

$$\bar{\Delta} = \lambda_1 E\left[Q_i\right] = \lambda_1 \left(E\left[X_i^1 Y_i\right] + E\left[\frac{1}{2}\left(X_i^1\right)^2\right] \right), \quad (6)$$

and

$$E\left[\frac{1}{2}\left(X_i^1\right)^2\right] = \frac{1}{\lambda_1^2}. \quad (7)$$

In practice, the average AoI increases when file is failed to decode during the transmission. As shown in Fig. 3(c), an additional areas Q_2' is resulted from the file 2 lost, then the area of trapezoid resulting from the lost file 2 can be expressed as:

$$Q_3^{(1)} = Q_3 + Q_2 + Q_2' = \frac{1}{2}\left(Y_3 + X_3^1 + X_2^1\right)^2 - \frac{1}{2}\left(Y_3\right)^2. \tag{8}$$

Therefore, let $Q_i^{(1)}$ denote the area of trapezoid caused by one file lost before we receive file i in the AoI evolution model, which can be expressed as:

$$\begin{aligned} Q_i^{(1)} &= Q_i + Q_{i-1} + Q_{i-1}' \\ &= \frac{1}{2}\left(Y_i + X_i^1 + X_{i-1}^1\right)^2 - \frac{1}{2}\left(Y_i\right)^2. \end{aligned} \tag{9}$$

More general, the areas resulting from n files lost before we receive file i can be expressed as:

$$Q_i^{(n)} = \sum_{j=0}^{n}\left[X_{i-j}^1 Y_i + \frac{1}{2}\left(X_{i-j}^1\right)^2\right] + \sum_{j=0}^{n}\sum_{l=0,l\neq j}^{n} X_{i-j}^1 X_{i-l}^1. \tag{10}$$

Let ε_{δ_1} and ε_{δ_2} denote the FER in the first- and second-hop transmission, then the reliable transmission probability of file i through dual-hop transmission can be denoted as:

$$\Xi(i) = \left(1-\varepsilon_{\delta_1}\right)\left(1-\varepsilon_{\delta_2}\right). \tag{11}$$

Note that the system time Y_i and the interval time X_i^1 are all stochastically identical, Thus, the time interval X_i^1, X_{i-1}^1 and Y_i in (9) are all independent. Since the transmission of each file is independent, and the reliable transmission probability of delivering a file is expressed in (11) and $\Xi(i) \in (0,1]$, the average AoI then can be expressed as $\lambda\sum_{n=0}^{\infty}\Xi(i)(1-\Xi(i))^n\mathbb{E}[Q_i^{(n)}]$. Therefore, combined with (10) and the properties of the Hypo-exponential distribution [33], the average AoI in our system can be further expressed as:

$$\begin{aligned} \bar{\Delta}_c &= \lambda\sum_{n=0}^{\infty}\Xi(i)(1-\Xi(i))^n\cdot\left(E\left[X_i^1 Y_i\right] + nE\left[X_{i-1}^1 Y_i\right]\right. \\ &\quad \left. + \frac{n+1}{2}E\left[\left(X_i^1\right)^2\right] + \binom{n}{2}E\left[X_i^1\right]^2\right) \\ &= \lambda E\left[X_i^1 Y_i\right] + \frac{1-\Xi(i)}{\Xi(i)}E\left[Y_i\right] \\ &\quad + \frac{1}{\lambda\Xi(i)} + \frac{1}{\lambda}\left(\frac{1-\Xi(i)}{\Xi(i)}\right)^2 \end{aligned} \tag{12}$$

From (12), we can find that the crucial part in the closed-form expression of average AoI is deriving $E[X_i^1 Y_i]$ and $E[Y_i]$, which can be further expressed as

$$E\left[Y_i\right] = E\left[W_i + T_i\right] = E\left[w_i^1 + w_i^2 + T_i^1 + T_i^2\right], \tag{13}$$

and

$$\begin{aligned} E\left[X_i^1 Y_i\right] &= E\left[X_i^1\left(W_i + T_i\right)\right] \\ &= E\left[X_i^1\left(w_i^1 + w_i^2 + T_i^1 + T_i^2\right)\right], \end{aligned} \tag{14}$$

where T_i^1 and T_i^2 are the end-to-end delay of the first- and second-hop, respectively.

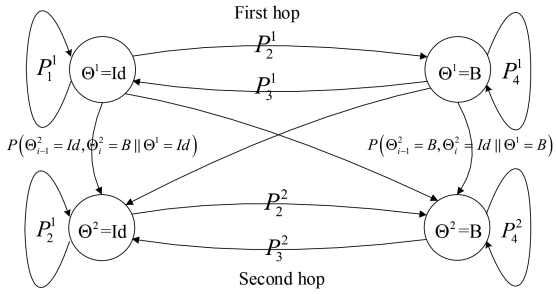

Fig. 4. 4-state Markov chain of the dual-hop transmission, where the first-hop is a two state Markov chain and the second-hop is also a two state Markov chain depends on the state of the first-hop.

We can construct two discrete Markov chains to analyze $E[X_i^1 Y_i]$ and $E[Y_i]$. Note that the independent variables w_i^1, w_i^2, T_i^1 and T_i^2 all follow the exponential distribution with mean value $1/\mu_\zeta, \zeta = 1, 2$.

Therefore, in the first-hop, when the file i steadily arrives at S, it may find S is in the state B or Id, which can be denoted as Θ_i^1, and we have $\Theta_i^1 = \{Id, B\}$. This can be established as a two-state Markov chain. In the second-hop, the state of R can also be denoted as $\Theta_i^2 = \{Id, B\}$, and the main difference is the interval time of the consecutive files arrival. Then, a 4-state Markov chain for the dual-hop transmission is illustrated in Fig. 8.

In detail, the arrival interval time of the first-hop is $X_i^1 = \frac{1}{\lambda_1}$. However, the arrival interval time of the second-hop depends on the state of the first-hop, which can be expressed as $X_i^2 = X_i^1 + Y_i^1 - Y_{i-1}^1$. Therefore, the average AoI for the first-hop transmission can be directly expressed as

$$\begin{aligned} \bar{\Delta}_1 &= \lambda_1\sum_{n=0}^{\infty}\Xi^1(i)\left(1-\Xi^1(i)\right)^n\cdot\left(E\left[X_i^1 Y_i^1\right] + nE\left[X_{i-1}^1 Y_i^1\right]\right. \\ &\quad \left. + \frac{n+1}{2}E\left[\left(X_i^1\right)^2\right] + \binom{n}{2}E\left[X_i^1\right]^2\right) \\ &= \lambda_1 E\left[X_i^1 Y_i^1\right] + \frac{1-\Xi^1(i)}{\Xi^1(i)}E\left[Y_i^1\right] \\ &\quad + \frac{1}{\lambda_1\Xi^1(i)} + \frac{1}{\lambda_1}\left(\frac{1-\Xi^1(i)}{\Xi^1(i)}\right)^2, \end{aligned} \tag{15}$$

where $\Xi^1(i) = 1 - \varepsilon_{\delta_1}$ represents the successful probability of file i in the first-hop transmission, and we have

$$\begin{aligned} E\left[X_i^1 Y_i^1\right] &= \left(\frac{1}{\lambda_1\mu_1} + \frac{\lambda_1}{\mu_1\left(\lambda_1+\mu_1\right)^2}\right)\lambda_1 \\ &\quad + \frac{2\lambda_1^2\mu_1^2}{\left(\lambda_1+\mu_1\right)^3\left(\lambda_1^2+\lambda_1\mu_1+\mu_1^2\right)} \end{aligned} \tag{16}$$

and

$$\begin{aligned} E\left[Y_i^1\right] &= E\left[Y_i^1 \mid K_{i-1}^1 = (B)\right]P_B^1 \\ &\quad + E\left[Y_i^1 \mid K_{i-1}^1 = (Id)\right]P_I^1 \end{aligned}$$

$$= \left[\frac{1}{\mu_1} + \frac{1}{\mu_1(\lambda_1+\mu_1)} + \frac{\lambda_1}{(\lambda_1+\mu_1)^2}\right]\frac{\mu_1^2}{\lambda_1^2+\lambda_1\mu_1+\mu_1^2} + \left[\frac{1}{\mu_1} + \frac{1}{\mu_1(\lambda_1+\mu_1)}\right]\frac{\lambda_1^2+\lambda_1\mu_1}{\lambda_1^2+\lambda_1\mu_1+\mu_1^2} \quad (17)$$

The expression of average AoI for dual-hop transmission in the closed-form is further derived as (18) shown at the bottom of this page, and the detailed derivation is given in Appendix B.

Moreover, for the peak AoI (PAoI), based on the definition in [14], we have

$$\bar{\Delta}_{PAoI} = E\left[X_{i^*} + Y_{i^*}\right], \quad (19)$$

where i^* is the latest file arriving at the queue in a given service period. Therefore, we have $E[X_{i^*}+Y_{i^*}] = \frac{E[X_i+Y_i\|_{i=i^*}]}{\Pr(i=i^*)}$, where $\|_{i=i^*}$ is the indicator function of whether a given file is the freshest in a given period, and $\Pr(i=i^*)$ refers to its probability. Similar to the above analysis of average AoI, we extend the PAoI to a practical case by considering the file loss, and we have

$$\bar{\Delta}_P = \sum_{n=0}^{\infty}\Xi(i)(1-\Xi(i))^n\cdot\left(E\left[nX_{i^*-1}+2X_{i^*}+Y_{i^*}\right]\right) = E\left[2X_{i^*}+Y_{i^*}\right] + \frac{(1-\Xi(i))}{\Xi(i)}E\left[X_{i^*-1}\right]. \quad (20)$$

By utilizing the 4-state Markov chain analysis, the closed-form expression of the PAoI for the first-hop can be expressed as

$$\bar{\Delta}_{P_1} = E\left[2X_{i^*}^1 + Y_{i^*}^1\right] + \frac{\left(1-\Xi^1(i)\right)}{\Xi^1(i)}E\left[X_{i^*-1}^1\right] = \left(\frac{2}{\lambda_1} + \frac{1}{\mu_1} + \frac{\lambda_1\left(\mu_1^2-\lambda_1^2-\lambda_1\mu_1\right)}{\mu_1(\lambda_1+\mu_1)\left(\lambda_1^2+\lambda_1\mu_1+\mu_1^2\right)} - \frac{\lambda_1\left(\lambda_1^2+\lambda_1\mu_1\right)}{(\lambda_1+\mu_1)^2\left(\lambda_1^2+\lambda_1\mu_1+\mu_1^2\right)}\right)\cdot\frac{\lambda_1^2+\lambda_1\mu_1+\mu_1^2}{\mu_1(\lambda_1+\mu_1)} + \frac{\left(1-\Xi^1(i)\right)}{\lambda_1\Xi^1(i)}. \quad (21)$$

The closed-form expression of the PAoI of dual-hop can be derived as (22) shown at the bottom of this page, and the derivation process can also be found in Appendix B.

C. End-to-End Delay and Throughput of Age-Optimal NC-HARQ Transmission Scheme

The end-to-end delay T_i^{ζ} contains the data buffering time, HARQ feedback delay, propagation delay and the decoding time in ζ-th hop transmission. Let T_{pack} denote the data buffering time, D_f denotes the HARQ feedback delay, T_{prop} denotes the propagation delay and $\mathbb{C}(\cdot)$ denotes the decoding time. Therefore, the end-to-end expected delay of the NCnr-HARQ and NCor-HARQ relay modes in the first-hop can be expressed as:

$$\tau_{NCnr}^1 = \chi T_{\text{pack}} + D_f + \delta_1 T_{\text{prop}} + \mathbb{C}\left(\delta_1\right), \quad (23)$$

and

$$\tau_{NCor}^1 = \chi T_{\text{pack}} + D_f + \delta_1 T_{\text{prop}} + \mathbb{C}\left(\delta_1\right) + \varepsilon_{\delta_1}\cdot\left(\left(\delta_{F_1}-\delta_1\right)T_{\text{prop}} + \mathbb{C}\left(\delta_{F_1}-\delta_1\right)\right), \quad (24)$$

$$\bar{\Delta} = \left(\frac{1}{\lambda_1\mu_1} + \frac{\lambda_1}{\mu_1(\lambda_1+\mu_1)^2}\right)\lambda_1 + \frac{2\lambda_1^2\mu_1^2}{(\lambda_1+\mu_1)^3\left(\lambda_1^2+\lambda_1\mu_1+\mu_1^2\right)} + \frac{1}{\mu_2} + \frac{\lambda_1^2\mu_1^3}{\mu_2(\lambda_1+\mu_1)(\lambda_1+\mu_2)^2(\mu_1-\mu_2)(\mu_1+\mu_2)}$$
$$\cdot\left(1+\frac{\lambda_1\mu_1(\lambda_1+2\mu_1)}{(\lambda_1+\mu_1)(\mu_1+\mu_2)(\mu_1-\mu_2)} + \frac{\mu_1^2}{(\lambda_1+\mu_1)(\mu_1-\mu_2)} + \frac{\lambda_1}{\mu_1+\mu_2}\right) + \frac{P_2^2}{1+P_2^2-P_4^2}\cdot\frac{\lambda_1^2\mu_1^3}{(\lambda_1+\mu_1)(\lambda_1+\mu_2)^2(\mu_1-\mu_2)(\mu_1+\mu_2)}$$
$$\left(\frac{2}{\lambda_1+\mu_2} - \frac{2\mu_2}{\mu_1^2-\mu_2^2} + \frac{2\lambda_1\mu_1(\lambda_1+2\mu_1)}{(\lambda_1+\mu_1)(\mu_1+\mu_2)(\mu_1-\mu_2)}\cdot\left(\frac{1}{\lambda_1+\mu_2} - \frac{2\mu_2}{\mu_1^2-\mu_2^2}\right) + \frac{\mu_1^2}{(\lambda_1+\mu_1)(\mu_1-\mu_2)}\cdot\left(\frac{2}{\lambda_1+\mu_2} - \frac{\mu_1+3\mu_2}{\mu_1^2-\mu_2^2}\right)\right.$$
$$\left. + \frac{\lambda_1}{\mu_1+\mu_2}\cdot\left(\frac{2}{\lambda_1+\mu_2} + \frac{\mu_1-3\mu_2}{\mu_1^2-\mu_2^2}\right)\right) + \frac{1}{\lambda\Xi(i)} + \frac{1}{\lambda}\left(\frac{1-\Xi(i)}{\Xi(i)}\right)^2 + \frac{1-\Xi(i)}{\Xi(i)}\cdot\frac{1+2P_2^2-P_4^2}{\mu_2\left(1+P_2^2-P_4^2\right)} \quad (18)$$

$$\bar{\Delta}_{PAOI} = \left(\frac{2}{\lambda_1} + \frac{1}{\mu_1} + \frac{\lambda_1\left(\mu_1^2-\lambda_1^2-\lambda_1\mu_1\right)}{\mu_1(\lambda_1+\mu_1)\left(\lambda_1^2+\lambda_1\mu_1+\mu_1^2\right)} - \frac{\lambda_1\left(\lambda_1^2+\lambda_1\mu_1\right)}{(\lambda_1+\mu_1)^2\left(\lambda_1^2+\lambda_1\mu_1+\mu_1^2\right)}\right)\frac{\lambda_1^2+\lambda_1\mu_1+\mu_1^2}{\mu_1(\lambda_1+\mu_1)}$$
$$+ \left(\frac{1}{\mu_2} + \frac{1}{\mu_2}P_2^2\right)\frac{1-P_4^2}{1+P_2^2-P_4^2-\left(P_2^2\right)^2} + \left(\frac{1}{\mu_2} - \frac{1}{\mu_2}\left(2P_2^2-P_4^2\right)\right)\frac{P_2^2}{1+P_2^2-P_4^2-\left(P_2^2\right)^2}$$
$$+ \frac{(1-\Xi(i))}{\lambda_1\Xi(i)} \quad (22)$$

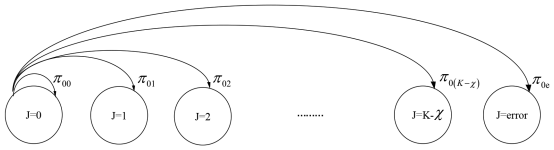

Fig. 5. Trellis diagram of the first-hop.

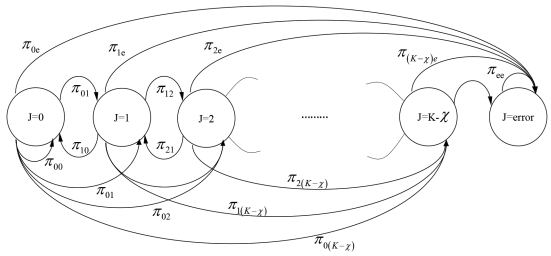

Fig. 6. Trellis diagram of the second-hop.

where δ_1 and ε_{δ_1} in (23) and (24) are the estimated δ_1 NC packets and FER after δ_1 NC packets transmission in the first-hop over the SR fading channel, which can be denoted as:

$$\begin{aligned}\delta &= \chi/\left(1-P_E\right)\\ &= \chi/\left(1-(1-P_e)^L\right)\\ &= \chi/\left(1-\left(\sum_{k=0}^{m-1}\alpha\theta_k\sum_{j=1}^{\max(M/4,1)}\frac{1}{\xi_M}\right.\right.\\ &\left.\left.\left(\frac{1}{\eta^{k+1}}-\frac{1}{\sqrt{2\pi}}\sum_{i=0}^{k}\frac{1}{i!}\frac{1}{2^{i-v}b_j^{2i}\eta^{k-i+1}\left(1+\eta/b_j^2\right)^v}\Gamma(v)\right)\right)^L\right),\end{aligned} \tag{25}$$

and

$$\varepsilon_\delta = C_\delta^\chi\sum_{i=1}^{\chi}(1-P_E)^{\chi-i}P_E^i, \tag{26}$$

where $P_E = 1-(1-P_e)^L$ is the packet error rate, L is the packet length. For the NCor-HARQ relay mode, S can get the precise CSI s_{δ_1} from the delayed feedback and prepare the one-time retransmission. Specifically, we can calculate δ_{F_1} for reliable transmission through substituting $Pe = Pe_{\delta_1}$ in (25). Then, we can set $Pe = Pe_{\delta_1}$ and $\delta = \delta_{F_1}$ in (26) to calculate $\varepsilon_{\delta_{F_1}}$ for (24), which is the FER after δ_{F_1} NC packets transmission.

The definition expression of throughput for the two relay modes in our age-optimal NC-HARQ transmission scheme is

$$T = \frac{\chi\left(1-\zeta_{NC}\right)}{\tau}, \tag{27}$$

where ζ_{NC} is the error probability in our age-optimal NC-HARQ transmission scheme, and τ is the expected transmission delay.

In our age-optimal NC-HARQ transmission scheme for the dual-hop satellite-integrated Internet communication scenario, we use two trellis diagrams to analyze throughput in the first-hop and second-hop as shown in Fig. 5 and Fig. 6. In Fig. 5, each state $J = j$ represents S has sent $K-j$ NC packets for the reliable transmission of a file, if R can successfully recover this file, R can re-encode at most $K+j$ NC packets to forward this file to D. Therefore, we can see that before the first-hop transmission, the system is at the state $J = 0$. After the first-hop transmission, the system could be at one of $K-\chi+2$ states including the $J = 0$ and error state. If the receiver fails to decode the messages after the first-hop transmission, then the system transits from state $J = i$ to the error state. The state transition matrix for the first-hop of our age-optimal NC-HARQ transmission scheme can be expressed as $P_1 = [\,\pi_{00},\ \pi_{01},\ \ldots,\pi_{0(K-\chi)},\ \pi_{0e}\,]$, where the transition probability π_{ij} is the probability of transiting from state $J = i$ to $J = j$, and we have $\pi_{0j} \approx \varepsilon_{K-j-1} - \varepsilon_{K-j}$, for $0 \le j \le K-\chi$, and $\pi_{0e} \approx \varepsilon_K$. Thus, we have:

$$\zeta_{NC}^1(K, K-\chi) = \varepsilon_K. \tag{28}$$

Similarly, Fig. 6 shows a trellis diagram of the second-hop age-optimal NC-HARQ transmission scheme. The system could in any state except $J = error$ at the beginning of the second-hop. Therefore, the transition matrix of the second-hop transmission can be expressed as:

$$P_2 = \begin{bmatrix} \pi_{00} & \cdots & \pi_{0(K-\chi)} & \pi_{0e}\\ \vdots & \cdots & \vdots & \vdots\\ \pi_{(K-\chi)0} & \cdots & \pi_{(K-\chi)(K-\chi)} & \pi_{(K-\chi)e}\\ 0 & \cdots & 0 & 0\end{bmatrix}. \tag{29}$$

Then, we suppose that the stationary probability distribution is $P_{\text{state}} = [\,a_0,\ a_1,\ \cdots\ a_{K-\chi+1}\,]$. Note that $P_{\text{state}}P_2 = P_{\text{state}}$, and we have:

$$\zeta_{NC}^2(K, K-\chi) = a_{K-\chi+1}. \tag{30}$$

Thus, we can express the total throughput of the dual-hop age-optimal NC-HARQ transmission scheme as:

$$T_{NC} = \frac{\chi\left(1-\varepsilon_K\right)\left(1-a_{K-\chi+1}\right)}{\tau}. \tag{31}$$

Thus, T_{NCnr} can be derived through letting $\tau = \tau_{NCnr}$, which is expressed as (32), and T_{NCor} can be derived through $\tau = \tau_{NCor}$, which is expressed as (33) shown at the bottom of the next page.

$$\begin{aligned}\tau_{NCnr} &= 2\chi T_{\text{pack}} + D_f + \delta_1 T_{\text{prop}}\\ &\quad + \mathbb{C}\left(\delta_1\right) + \delta_2 T_{\text{prop}} + \mathbb{C}\left(\delta_2\right).\end{aligned} \tag{32}$$

Furthermore, the dynamic upper limit K_d of NC packets can be expressed as:

$$K_d = \sum_{i=0}^{K-\chi+1} a_i\pi_{ie}(K+i) + \sum_{i=0}^{K-\chi+1}\sum_{j=0}^{K-\chi} a_i\pi_{ij}(K+i-j). \tag{34}$$

D. End-to-End Delay and Throughput of Fast HARQ

In the Fast HARQ transmission protocol [24], the end-to-end expected delay in our dual-hop satellite-integrated Internet

scenario can be denoted as

$$\tau_{\text{fast}} = \chi T_{\text{pack}} + \sum_{\delta=1}^{K} \Pr\left(G \in s^{\delta}\right) \left(\delta T_{\text{prop}} + \mathbb{C}(\delta)\right) + \sum_{\delta=1}^{K-1} \sum_{i=\delta+1}^{K} \left(T_{\text{prop}} + \mathbb{C}(i)\right) \theta_{i-1}^{\delta} + D_f \left(1 + \sum_{\delta=1}^{K-1} \Pr\left(G \in s^{\delta}\right) + \sum_{\delta=1}^{K-1} \sum_{i=\delta+1}^{K} \theta_{i-1}^{\delta}\right), \tag{35}$$

where

$$\Pr\left(G \in s^{\delta}\right) = \int_{q^{\delta}}^{q^{\delta-1}} f_{SR}(x) dx, \tag{36}$$

and

$$\theta_i^{\delta} = \int_{q^{\delta}}^{q^{\delta-1}} f_{SR}(x) Q\left(\frac{\sqrt{i}\left(\log(1+x) - \frac{\chi}{i}\right)}{\sqrt{1 - \frac{1}{(1+x)^2}}}\right) dx, \tag{37}$$

and $f_{SR}(x)$ can be obtained in (1).

The throughput of Fast HARQ protocol can be expressed as

$$\eta_{\text{Fast}} = \frac{\chi(1 - \Pr(\text{error}))}{\tau_{\text{fast}}}, \tag{38}$$

where

$$\Pr(\text{error}) = \int_{0}^{\infty} f_{SR}(x) Q\left(\frac{\sqrt{K}\left(\log(1+x) - \frac{\chi}{K}\right)}{\sqrt{1 - \frac{1}{(1+x)^2}}}\right) dx. \tag{39}$$

Therefore, as for the analysis of the average AoI and PAoI of Fast HARQ, we can substitute (35) and (39) which can be seen as the end-to-end delay and FER into (18) and (22), respectively.

E. End-to-End Delay and Throughput of D-HARQ

The expected end-to-end delay of the D-HARQ transmission protocol [25] in our dual-hop satellite-integrated Internet scenario can be denoted as

$$\tau_{Dynamic} = \chi T_{\text{pack}} + \chi P'_{\text{state}} (\Pi \circ \Upsilon) \mathrm{T}_{m+2} \left(T_{\text{prop}} + D_f + \mathbb{C}\right), \tag{40}$$

where

$$\Pi = \begin{bmatrix} \pi_{00} & \cdots & \pi_{0\tilde{}m} & \pi_{0e} \\ \vdots & \cdots & \vdots & \vdots \\ \pi_{m0} & \cdots & \pi_{mm} & \pi_{me} \\ \pi_{e0} & \cdots & \pi_{em} & \pi_{ee} \end{bmatrix}, \tag{41}$$

TABLE I
SHADOWED-RICIAN FADING PARAMETERS

Shadowing	b_i	Ω_i	m_i
Infrequent light shadowing (ILS)	0.158	1.29	20
Average shadowing (AS)	0.126	0.835	11
Frequent heavy shadowing (FHS)	0.063	0.000897	1

and

$$\pi_{ij} \approx \begin{bmatrix} \varepsilon_{K-j+i-1} - \varepsilon_{K-j+i}, 0 \le j < m \\ 1 - \varepsilon_{K+i-m}, j = m \\ 0, \text{ otherwise} \end{bmatrix}, \tag{42}$$

and

$$\Upsilon = \begin{bmatrix} K & K-1 & \cdots & K-m & K \\ K+1 & K & \cdots & K-m+1 & K+1 \\ \vdots & \vdots & \cdots & \vdots & \vdots \\ K+m & K+m-1 & \cdots & K & K+m \\ K & K-1 & \cdots & K-m & K \end{bmatrix}, \tag{43}$$

and $\Pi \circ Y$ is the Hadamard product. Moreover, the throughput of D-HARQ can be denoted as

$$\eta_{Dynamic} \approx \frac{\chi\left(1 - \zeta_{Dynamic}\right)}{2nP'_{\text{state}} \left(\Pi^{\circ} \Lambda\right) \mathbf{1}_{m+2}}. \tag{44}$$

Similarly, based on the average AoI and PAoI analysis of NCnr-HARQ, NCor-HARQ and Fast HARQ, we can substitute the end-to-end delay and FER into (18) and (22) to derive the average AoI and PAoI, respectively.

IV. SIMULATION RESULTS AND DISCUSSIONS

In this section, we present the theoretical and Monte Carlo simulation results to evaluate the performance of our dual-hop age-optimal NC-HARQ transmission scheme, and compare with the Fast HARQ [24] and D-HARQ [25]. First, we simulate the NCnr-HARQ and NCor-HARQ relay modes in different SR fading parameters to show the effectiveness of our age-optimal NC-HARQ transmission scheme, and the fading parameters of infrequent light shadowing (ILS), average shadowing (AS) and frequent heavy shadowing (FHS) are summarized in Table I. The rest of simulation parameters are shown in Table II.

First, we present the Monte Carlo simulation results of BER over SR fading channel with FHS, AS and ILS parameters from Table I as shown in Fig. 7(a), and verify the accuracy of (2). In Fig. 7(b), we present the simulation result of stationary probabilities of good and bad states based on a threshold $r_t = 5$ dB and validate the accuracy of (3) and (4).

In Fig. 8(a), we compare the simulation of our derived closed-form BER expression in (2) with the related expression (38) in [35], which validates the accuracy of our derivation to the BER of SR fading channel. Further, in order to validate the age-optimal NC-HARQ transmission scheme can enhance the

$$\tau_{NCor} = 2\chi T_{\text{pack}} + 2D_f + \delta_1 T_{\text{prop}} + \mathbb{C}\left(\delta_1\right) + \varepsilon_{\delta_1} \cdot \left(\left(\delta_{F_1} - \delta_1\right) T_{\text{prop}} + \mathbb{C}\left(\delta_{F_1} - \delta_1\right)\right) + \delta_2 T_{\text{prop}} + \mathbb{C}\left(\delta_2\right) + \varepsilon_{\delta_2} \cdot \left(\left(\delta_{F_2} - \delta_2\right) T_{\text{prop}} + \mathbb{C}\left(\delta_{F_2} - \delta_2\right)\right) \tag{33}$$

TABLE II
SIMULATION PARAMETERS

Parameter	Value
The SR fading parameter in the second-hop	b_0 = 0.053
Bandwidth	B = 400 MHz
Path loss exponent	α = 2.5
Noise density	N_0 = -174 dBm/Hz
The constant coefficient associated with the power amplifier	A = 2
Distance	d = 600 km
Feedback signal propagation delay	D = 2 ms
Packet processing delay	$\mathbb{C}(1)$ = 0.25 ms
Packet data buffering time	T_{pack} = 2.5 ms
Data transmission rate	R_{data} = 100 Mbit/s
File size	F_s = 4 kbyte

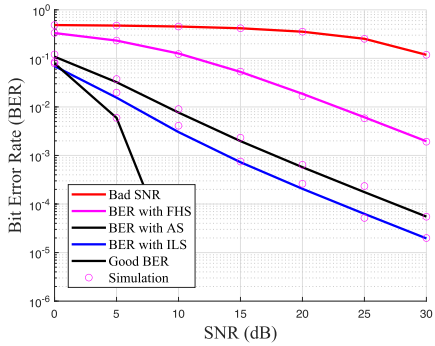

(a)

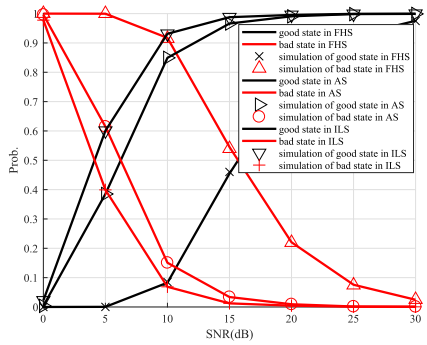

(b)

Fig. 7. The derived BER of SR fading channel under FHS, AS and ILS fading parameters, and the stationary probabilities of good and bad states with a threshold r_t = 5 dB. (a) BER versus different fading parameters. (b) Stationary probabilities versus average SNR.

reliability with physical layer error control techniques in the dual-hop satellite-integrated Internet transmission, we utilize the FEC and modulations in DVB-S2 to our age-optimal NC-HARQ transmission scheme [34], and also change the number of redundant packets K in two relay modes. The Monte Carlo simulation result in Fig. 8(b) shows that our NCnr-HARQ and NCor-HARQ relay modes have great potential to improve the BER with powerful FEC in DVB-S2, and by increasing the number of redundant packets. Note that the uncoded NCnr-HARQ scheme with $K = 0$ is only transmitting the information bit, thus it has the same BER performance as the SR fading channel with FHS in Fig. 8(a), and we discuss the effects of K in the later simulations. Moreover, the concatenated FEC consists of an outer BCH code

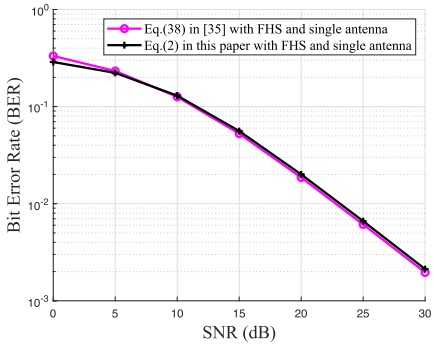

(a)

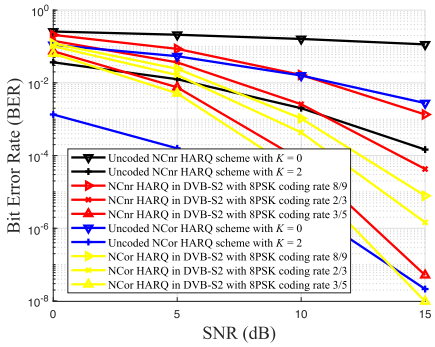

(b)

Fig. 8. The end-to-end BER performance under SR fading channel with FHS, and our NCnr-HARQ and NCor-HARQ modes with FEC in DVB-S2. (a) The derived BER of SR fading channel. (b) BER performance comparison of NCnr-HARQ and NCor-HARQ with FEC in DVB-S2.

and an inner LDPC code, and the total length of code block is 64800 bits, and the simulated code rates are 3/5, 2/3 and 8/9. In addition, each code block follows an interleaver with 21600 rows and 3 columns before the 8PSK modulation. As shown in Fig. 8(b), the end-to-end BER of NCnr-HARQ and NCor-HARQ can be decreased to about 10^{-8} at 15 dB, when we utilize a standardization 3/5 concatenated FEC with 8PSK in DVB-S2. Thus, to clearly reveal the difference and advantage of our proposed NCnr-HARQ and NCor-HARQ modes than other related HARQ schemes in dual-hop satellite-integrated Internet transmission, we simulate the age-optimal NC-HARQ transmission scheme itself without the DVB-S2 in the following comparisons.

In Fig. 9, the Monte Carlo simulation result shown that the NCor-HARQ mode can decrease the BER faster than that of NCnr-HARQ mode as well as the SNR increases under FHS. In addition, as aforementioned, the NCnr-HARQ with $K = 0$ means that there is no redundant packet during the transmission, thus, the BER of NCnr-HARQ with $K = 0$ equals to the BER of SR fading channel. On contrast, the NCor-HARQ relay mode has one-time retransmission, which can significantly lower the BER as shown in both Fig. 9(a) and Fig. 9(b). Moreover, the BER of NCor-HARQ mode is significantly lower than that of NCnr-HARQ mode under both ILS and AS fading levels, which means the NCor-HARQ mode can greatly improve the BER performance if the channel fading is not heavy. Thus,

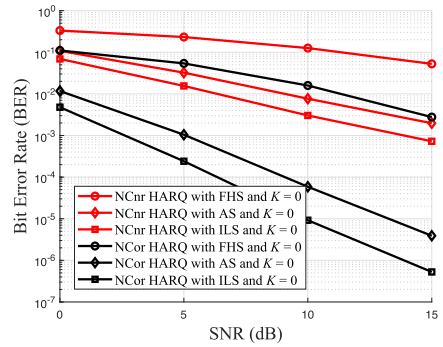

(a)

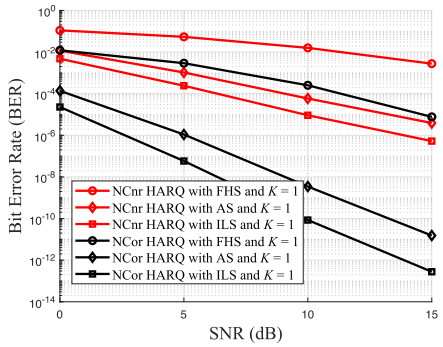

(b)

Fig. 9. BER of NCnr-HARQ and NCor-HARQ modes under FHS, ILS and AS SR fading parameters, (a) without redundant packet, and (b) with one redundant packet.

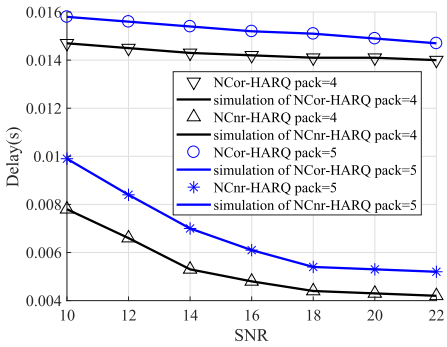

Fig. 10. The single-hop expected delay of NCnr-HARQ, NCor-HARQ with different number of packets.

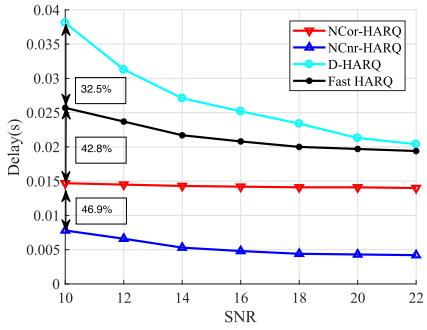

(a)

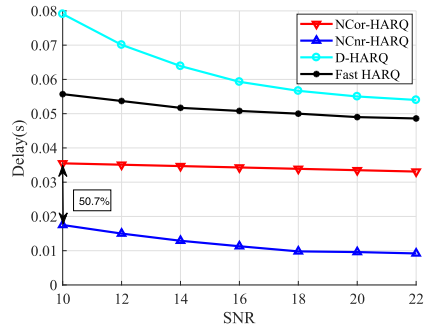

(b)

Fig. 11. The single-hop and dual-hop expected delay of NCnr-HARQ, NCor-HARQ, Fast HARQ, D-HARQ with respect to SNR. (a) Single-hop expected delay versus transmission SNR. (b) Dual-hop expected delay versus transmission SNR.

to show the difference clearly of our proposed NCnr-HARQ and NCor-HARQ modes in dual-hop satellite-integrated Internet transmission, we use the FHS parameters in the rest simulations.

In Fig. 10, we present the Monte Carlo simulation results to validate the accuracy of theoretical derivations of end-to-end expected delay under NCnr-HARQ and NCor-HARQ modes in (23) and (24), respectively. It is worth noting that the single-hop end-to-end expected delay of NCnr-HARQ mode is significantly lower than that of NCor-HARQ due to the one-time retransmission. We can further observe that when the SNR increases or the number of packets decreases, the delay of both NCnr-HARQ and NCor-HARQ decrease uniformly.

Next, we provide the Monte Carlo simulation results of expected delay for our NCnr-HARQ and NCor-HARQ modes, and compare to the Fast-HARQ and D-HARQ schemes under single-hop and dual-hop transmissions in Fig. 11 and Fig. 12 with respect to different SNR and BER, respectively. We can observe that the proposed age-optimal NC-HARQ transmission schemes have lower end-to-end delay than that of the Fast HARQ and D-HARQ schemes, and the NCnr-HARQ mode has the lowest end-to-end delay. Specially, our proposed NCnr-HARQ mode results in 46.9% relative end-to-end expected delay gain in the single-hop transmission compared with the NCor-HARQ mode. Moreover, in the dual-hop transmission, the end-to-end expected delay gain rises to 50.7%, which obviously illustrates the higher efficiency of our dual-hop age-optimal NC-HARQ transmission scheme. The main reason is that the NC packets in our age-optimal NC-HARQ transmission scheme can help to reduce the feedback and retransmissions as the LEC than the Fast HARQ and D-HARQ schemes. Moreover, the NCor-HARQ relay mode performs one-time retransmission when any packet is lost, which would cause a significant higher end-to-end delay than that of the NCnr-HARQ relay mode due the non-trivial propagation latency from S to R and D.

In Fig. 13, we provide the Monte Carlo simulation results of end-to-end dual-hop average AoI and PAoI versus SNR for our NCnr-HARQ and NCor-HARQ modes, and compare to the Fast-HARQ and D-HARQ schemes. We also verify the accuracy of closed-form expressions of average AoI and PAoI for

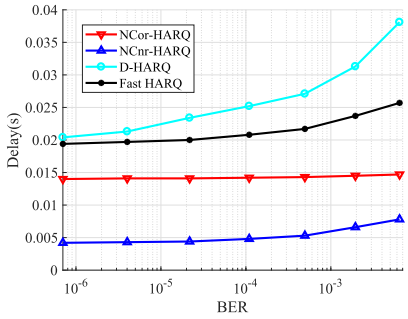

(a)

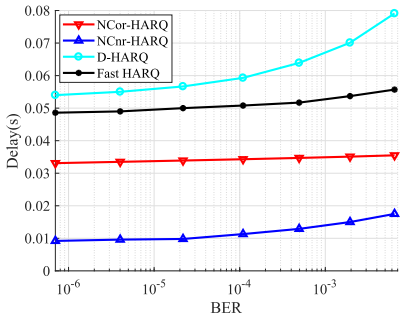

(b)

Fig. 12. The single-hop and dual-hop expected delay of NCnr-HARQ, NCor-HARQ, Fast HARQ and D-HARQ schemes with respect to BER. (a) Single-hop expected delay versus transmission BER. (b) Dual-hop expected delay versus transmission BER

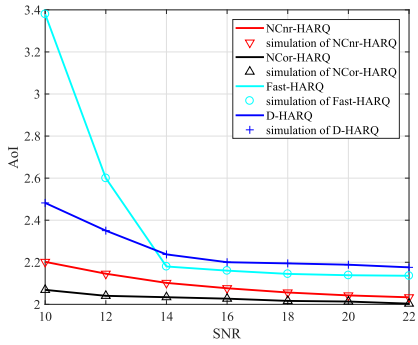

(a)

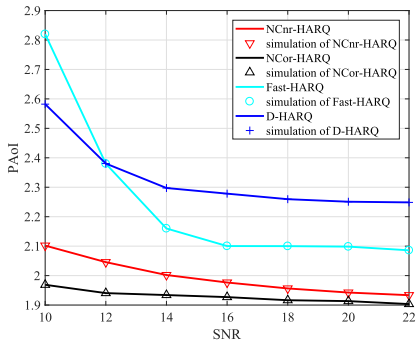

(b)

Fig. 13. Dual-hop average AoI, PAoI of NCnr-HARQ, NCor-HARQ, Fast HARQ and D-HARQ schemes with respect to SNR. (a) Dual-hop average AoI versus transmission SNR. (b) Dual-hop average PAoI versus transmission SNR.

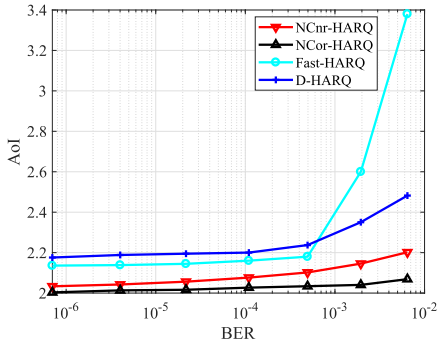

(a)

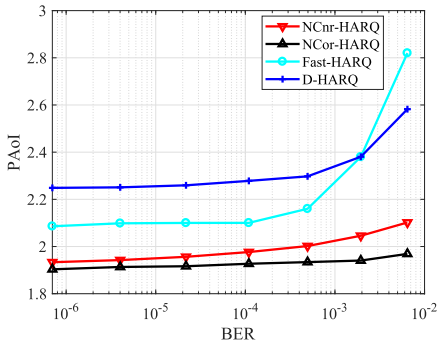

(b)

Fig. 14. Dual-hop average AoI, PAoI of NCnr-HARQ, NCor-HARQ, Fast HARQ and D-HARQ schemes with respect to BER. (a) Dual-hop average AoI versus transmission BER. (b) Dual-hop average PAoI versus transmission BER

under NCnr-HARQ and NCor-HARQ modes in (18) and (22), respectively. As shown in Fig. 13, our age-optimal NC-HARQ transmission scheme has remarkable superiority on both of the average AoI and PAoI than that of the Fast HARQ and D-HARQ schemes, especially when the SNR is less than 14 dB.

Moreover, we provide these Monte Carlo simulation results of average AoI and PAoI for the NCnr-HARQ and NCor-HARQ with respect to different BER in Fig. 14, which clearly shows the effect of end-to-end BER on the average AoI and PAoI. Note that the NCor-HARQ achieves better performance than the NCnr-HARQ in both average AoI and PAoI. This is because if S and R perform NCnr-HARQ mode, and R or D fails to decode with the under estimated NC packets due to the bad channel condition, this file would be discarded and cause a higher average AoI and PAoI, which leads D to wait for another successful transmission to update the AoI.

We compare the throughput performance of our age-optimal NC-HARQ transmission scheme with the Fast HARQ and D-HARQ schemes in Fig. 15 in the end-to-end dual-hop satellite-integrated Internet communication scenario. Similarly, our age-optimal NC-HARQ transmission can utilize the NC packets as the LEC to reduce the feedback and retransmissions, which can achieve lower end-to-end delay to increase the throughput than the Fast HARQ and D-HARQ schemes. Last but not least, the NCnr-HARQ relay mode has the highest throughput as shown in Fig. 15, this is because R and D with

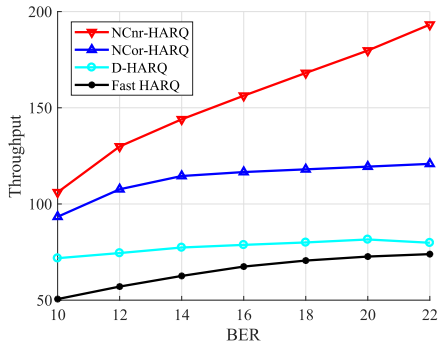

Fig. 15. The throughput of NCnr-HARQ, NCor-HARQ, Fast HARQ and D-HARQ schemes with respect to SNR.

NCnr-HARQ mode could receive more packets in the same end-to-end delay without waste the non-trivial propagation latency for the one-time retransmission in the NCor-HARQ mode.

V. Conclusion

In this paper, we have proposed an age-optimal NC-HARQ transmission scheme in the dual-hop satellite-integrated Internet communication scenario to improve the AoI, end-to-end delay and throughput metric compared with the state-of-the-art HARQ transmission schemes. We modeled the dual-hop satellite-integrated Internet transmission as a two-hop tandem queue, and introduced the age-optimal NC-HARQ transmission scheme in the dual-hop tandem queue in detail. Then, we established the AoI evolution models under the situation of single-hop and dual-hop transmission, and derived the closed-form expressions of AoI through setting up two-state and four-state Markov chains. Moreover, we analyzed the end-to-end delay and throughput of our age-optimal NC-HARQ transmission scheme, and compared to the Fast HARQ and D-HARQ schemes. Simulation results validated the accuracy of the derived expressions and showed that our proposed age-optimal NC-HARQ transmission scheme has better performance than the existing schemes.

Appendix A
Derivation of BER Expression in SR Fading Channel

In this section, we derive the BER expression (2) of the SR fading channel. Firstly, the BER of M-PSK with instant SNR r can be expressed as follows [31], [35],

$$P_e(r) = \frac{2}{\xi_M} \sum_{j=1}^{\max(M/4,1)} Q\left(\sqrt{2r}b_k\right), \tag{45}$$

where $\xi_M = \max(\log_2 M, 2)$ and $b_k = \sin\frac{(2k-1)\pi}{M}$.

Then, based on the PDF of SR fading distribution in (1) and the BER of M-PSK in (45), the BER of the SR fading channel can be derived through calculate $P_e = \int f(r)P_e(r)dr$, and we have:

$$\begin{aligned} P_e &= \int f(r)P_e(r)dr \\ &= \int \frac{2}{\xi_M} \sum_{j=1}^{\max(M/4,1)} Q\left(\sqrt{2r}b_k\right) \cdot \frac{1}{2b_0\gamma}\left(\frac{2b_0m}{2b_0m+\Omega}\right)^m \\ &\quad \cdot \exp\left(-\frac{r}{2b_0\gamma}\right) \cdot {}_1F_1\left(m, 1, \frac{1}{2b_0\gamma}\left(\frac{\Omega}{(2b_0m+\Omega)}\right)r\right)dr, \end{aligned} \tag{46}$$

where

$$\begin{aligned} &{}_1F_1\left(m; 1; \frac{1}{2b_0\gamma}\left(\frac{\Omega}{(2b_0m+\Omega)}\right)r\right) \\ &= \exp\left(\frac{1}{2b_0\gamma}\left(\frac{\Omega}{(2b_0m+\Omega)}\right)r\right) \\ &\quad \times \sum_{1}^{m-1} \frac{(-1)^k(1-m)_k\left(\frac{1}{2b_0\gamma}\left(\frac{\Omega}{(2b_0m+\Omega)}\right)r\right)^k}{(k!)^2}. \end{aligned} \tag{47}$$

Therefore, we have

$$\begin{aligned} P_e &= \int f(r)P_e(r)dr \\ &= \int_0^\infty \sum_{k=0}^{m-1} \alpha e^{-\eta r}\theta_k \frac{r^k}{k!} \\ &\quad \times \int_{\sqrt{2\gamma}b_j}^\infty \frac{2}{\xi_M} \sum_{j=1}^{\max(M/4,1)} \frac{1}{\sqrt{2\pi}} e^{-\frac{t^2}{2}} dtdr \\ &= \int_0^\infty \frac{2}{\xi_M} \sum_{j=1}^{\max(M/4,1)} \frac{1}{\sqrt{2\pi}} e^{-\frac{t^2}{2}} \\ &\quad \times \int_0^{\frac{t^2}{2b_j^2}} \sum_{k=0}^{m-1} \alpha e^{-\eta r}\theta_k \frac{r^k}{k!} drdt, \end{aligned} \tag{48}$$

where $\theta_k = \frac{(-1)^k(1-m)_k}{k!}\left(\frac{1}{2b_0\gamma}\frac{\Omega}{2b_0m+\Omega}\right)^k$. Thus, we can finally get the derivation of BER in SR fading channel as follows:

$$\begin{aligned} p_e &= \int_0^\infty \frac{2}{\xi_M} \sum_{j=1}^{\max(M/4,1)} \frac{1}{\sqrt{2\pi}} e^{-\frac{t^2}{2}} \sum_{k=0}^{m-1} \alpha\theta_k \\ &\quad \left(\frac{1}{\eta^{k+1}} - e^{-\frac{\eta t^2}{2b_j^2}} \sum_{i=0}^{k} \frac{1}{i!} \frac{t^{2i}}{2^i b_j^{2i} \eta^{k-i+1}}\right) dt \\ &= \sum_{k=0}^{m-1} \alpha\theta_k \sum_{j=1}^{\max(M/4,1)} \frac{1}{\xi_M} \\ &\quad \left(\frac{1}{\eta^{k+1}} - \frac{1}{\sqrt{2\pi}} \sum_{i=0}^{k} \frac{1}{i!} \frac{1}{2^{i-v} b_j^{2i} \eta^{k-i+1} \left(1+\eta/b_j^2\right)^v} \Gamma(v)\right), \end{aligned} \tag{49}$$

where $\alpha = \frac{1}{2b_0\gamma}\left(\frac{2b_0m}{2b_0m+\Omega}\right)^m$, $\eta = \frac{m}{(2b_0m+\Omega)\gamma}$, $v = \frac{2i+1}{2}$ and Γ is the Gamma function.

APPENDIX B
DERIVATION CLOSED-FORM EXPRESSIONS OF AVERAGE AOI AND PEAK AOI

In this section, we derive the average AoI expression (18) and average peak AoI expression (22) in closed-form through using the four-state Markov chain in Fig. 6. First, we obtain the transition probabilities for the first-hop:

$$P_2^1 = \Pr\left[\Theta_i^1 = (B) \mid \Theta_{i-1}^1 = (Id)\right] = \Pr\left[X_i^1 < T_{i-1}^1\right] = \frac{\lambda_1}{\lambda_1+\mu_1}, \tag{50}$$

and

$$P_4^1 = \Pr\left[\Theta_i^1 = (B) \mid \Theta_{i-1}^1 = (B)\right] = \Pr\left[X_i^1 < w_{i-1}^1 + T_{i-1}^1\right] = \frac{\lambda_1(\lambda_1+2\mu_1)}{(\lambda_1+\mu_1)^2}, \tag{51}$$

and

$$P_1^1 = 1 - \Pr\left(X_i^1 < T_{i-1}^1\right) = 1 - \frac{\lambda_1}{\lambda_1+\mu_1}, \tag{52}$$

and

$$P_3^1 = 1 - \Pr\left(X_i^1 < T_{i-1}^1 + w_{i-1}^1\right) = 1 - \frac{\lambda_1(\lambda_1+2\mu_1)}{(\lambda_1+\mu_1)^2}. \tag{53}$$

The state-transition matrix can be denoted as:

$$\Upsilon(1) = \begin{bmatrix} P_1^1 & P_2^1 \\ P_3^1 & P_4^1 \end{bmatrix} = \begin{bmatrix} \frac{\mu_1}{\lambda_1+\mu_1} & \frac{\lambda_1}{\lambda_1+\mu_1} \\ \left(\frac{\mu_1}{\lambda_1+\mu_1}\right)^2 & \frac{\lambda_1(\lambda_1+2\mu_1)}{(\lambda_1+\mu_1)^2}. \end{bmatrix} \tag{54}$$

The stationary probabilities can be calculated as $P_I^1 = \frac{\mu_1^2}{\lambda_1^2+\lambda_1\mu_1+\mu_1^2}P_B^1 = \frac{\lambda_1^2+\lambda_1\mu_1}{\lambda_1^2+\lambda_1\mu_1+\mu_1^2}$ where $P_I^1 = \Pr[\Theta_i^1 = (Id)]$, $P_B^1 = \Pr[\Theta_i^1 = (B)]$.

Similarly, the transition probabilities for the second-hop are derived as (55) and (56), both shown at the bottom of the page.

The state-transition matrix of the second-hop is $\Upsilon(2) = \begin{bmatrix} P_1^2 & P_2^2 \\ P_3^2 & P_4^2 \end{bmatrix}$. The stationary probabilities are denoted as $P_B^2 = \frac{P_2^2}{1+P_2^2-P_4^2}, P_I^2 = \frac{1-P_4^2}{1+P_2^2-P_4^2}$.

Recall (15) and (16) can be further expressed as:

$$\begin{aligned} E[X_iY_i] =& \left(E\left[X_i^1Y_i^1\right] + E\left[X_i^1Y_i^2\right]\right) \\ =& \left(E\left[X_i^1Y_i^1 \mid K_{i-1}^1 = (B)\right]\cdot P_B^1\right. \\ &+E\left[X_i^1Y_i^1 \mid K_{i-1}^1 = (Id)\right]\cdot P_I^1\big) \\ &+\left(E\left[X_i^1Y_i^2 \mid K_{i-1}^2 = (B)\right]\cdot P_B^2\right. \\ &+E\left[X_i^1Y_i^2 \mid K_{i-1}^2 = (Id)\right]\cdot P_I^2\big), \end{aligned} \tag{57}$$

and

$$\begin{aligned} E[Y_i] =& \left(E\left[Y_i^1\right] + E\left[Y_i^2\right]\right) \\ =& \left(E\left[Y_i^1 \mid K_{i-1}^1 = (B)\right]\cdot P_B^1\right. \\ &+E\left[Y_i^1 \mid K_{i-1}^1 = (Id)\right]\cdot P_I^1\big) \\ &+\left(E\left[Y_i^2 \mid K_{i-1}^2 = (B)\right]\cdot P_B^2\right. \\ &+E\left[Y_i^2 \mid K_{i-1}^2 = (Id)\right]\cdot P_I^2\big). \end{aligned} \tag{58}$$

First, we analyze $E[X_i^1Y_i^\zeta \mid \Theta_{i-1}^\zeta = (Id/B)]$ in the first-hop. When $\Theta_{i-1}^\zeta = Id$ and $\zeta = 1$, if $X_i^1 > T_{i-1}^1$ then $Y_i^1 = T_i^1$ and if $X_i^1 < T_{i-1}^1$ then $Y_i^1 = T_i^1 + w_i^1$. Therefore, we have

$$\begin{aligned} E\left[X_i^1Y_i^1 \mid \Theta_{i-1}^1 = (Id)\right] &= E\left[X_i^1T_i^1\right] + E\left[X_i^1w_i^1\big|_{X_i^1<T_{i-1}^1}\right] \\ &= E\left[X_i^1\right]E\left[T_i^1\right] + E\left[X_i^1w_i^1e^{-\mu_1X_i^1}\right] \\ &= \frac{1}{\lambda_1\mu_1} + \frac{\lambda_1}{\mu_1(\lambda_1+\mu_1)^2}. \end{aligned} \tag{59}$$

$$\begin{aligned} P_2^2 =& \Pr\left[\Theta_i^2 = (B) \mid \Theta_{i-1}^2 = (Id)\right] \\ =& \Pr\left[X_i^1 + T_i^1 - T_{i-1}^1 < T_{i-1}^2\right]P_1^1 + \Pr\left[X_i^1 + T_i^1 + w_i^1 - T_{i-1}^1 - w_{i-1}^1 < T_{i-1}^2\right]P_4^1 \\ &+ \Pr\left[X_i^1 + T_i^1 - T_{i-1}^1 - w_{i-1}^1 < T_{i-1}^2\right]P_3^1 + \Pr\left[X_i^1 + T_i^1 + w_i^1 - T_{i-1}^1 < T_{i-1}^2\right]P_2^1 \\ =& \frac{\lambda_1\mu_1^3}{(\lambda_1+\mu_2)(\mu_1+\mu_2)(\mu_1-\mu_2)(\lambda_1+\mu_1)} + \frac{\lambda_1^2\mu_1^4(\lambda_1+2\mu_1)}{(\lambda_1+\mu_2)(\mu_1+\mu_2)^2(\mu_1-\mu_2)^2(\lambda_1+\mu_1)^2} \\ &+ \frac{\lambda_1\mu_1^5}{(\lambda_1+\mu_2)(\mu_1+\mu_2)(\mu_1-\mu_2)^2(\lambda_1+\mu_1)^2} + \frac{\lambda_1^2\mu_1^3}{(\lambda_1+\mu_2)(\lambda_1+\mu_1)(\mu_1-\mu_2)(\mu_1+\mu_2)^2} \end{aligned} \tag{55}$$

$$\begin{aligned} P_4^2 =& \Pr\left[\Theta_i^2 = (B) \mid \Theta_{i-1}^2 = (B)\right] \\ =& \frac{\lambda_1\mu_1^3}{(\lambda_1+\mu_2)(\mu_1+\mu_2)(\mu_1-\mu_2)(\lambda_1+\mu_1)}\left(\frac{\mu_2}{\lambda_1+\mu_2} + \frac{\mu_1^2-3\mu_2^2}{\mu_1^2-\mu_2^2}\right) + \frac{\lambda_1^2\mu_1^4(\lambda_1+2\mu_1)}{(\lambda_1+\mu_1)^2(\lambda_1+\mu_2)(\mu_1-\mu_2)^2(\mu_1+\mu_2)^2} \\ &\left(\frac{\mu_1^2-5\mu_2^2}{\mu_1^2-\mu_2^2} + \frac{\mu_2}{\lambda_1+\mu_2}\right) + \frac{\lambda_1\mu_1^5}{(\lambda_1+\mu_2)(\mu_1+\mu_2)(\mu_1-\mu_2)^2(\lambda_1+\mu_1)^2} \\ &\left(\frac{\mu_2}{\lambda_1+\mu_2} + \frac{\mu_1^2-4\mu_2^2-\mu_1\mu_2}{\mu_1^2-\mu_2^2}\right) + \frac{\lambda_1^2\mu_1^3}{(\lambda_1+\mu_2)(\lambda_1+\mu_1)(\mu_1-\mu_2)(\mu_1+\mu_2)^2}\left(\frac{\mu_2}{\lambda_1+\mu_2} + \frac{\mu_1^2+\mu_1\mu_2-4\mu_2^2}{\mu_1^2-\mu_2^2}\right) \end{aligned} \tag{56}$$

When $\Theta_{i-1}^{\zeta}=B$ and $\zeta=1$, we have

$$\begin{aligned}
&E\left[X_i^1Y_i^1 \mid \Theta_{i-1}^1=(B)\right]\\
&=E\left[X_i^1T_i^1\right]+E\left[X_i^1w_i^1\big|_{X_i^1<T_{i-1}^1+w_i^1}\right]\\
&=E\left[X_i^1\right]E\left[T_i^1\right]+E\left[X_i^1w_i^1\left(e^{-\mu_1X_i^1}+\mu_1X_i^1e^{-\mu_1X_i^1}\right)\right]\\
&=\frac{1}{\lambda_1\mu_1}+\frac{\lambda_1}{\mu_1\left(\lambda_1+\mu_1\right)^2}+\frac{2\lambda_1}{\left(\lambda_1+\mu_1\right)^3}. \qquad (60)
\end{aligned}$$

Then, we analyze the second-hop ($\zeta=2$). When $\Theta_{i-1}^{\zeta}=Id$ and $\zeta=2$, if $X_i^2>T_{i-1}^2$ then $Y_i^2=T_i^2$ and if $X_i^2<T_{i-1}^2$ then $Y_i^2=T_i^2+w_i^2$. Therefore, we have

$$\begin{aligned}
&E\left[X_i^1Y_i^2 \mid \Theta_{i-1}^2=(Id)\right]\\
&=E\left[X_i^1T_i^2\right]+E\left[X_i^1w_i^2\big|_{X_i^2<T_{i-1}^2}\right]\\
&=E\left[X_i^1\right]E\left[T_i^2\right]+E\left[X_i^1w_i^2e^{-\mu_2X_i^2}\right]\\
&=\frac{1}{\mu_2}+\frac{\lambda_1^2\mu_1^3}{\mu_2\left(\lambda_1+\mu_1\right)\left(\lambda_1+\mu_2\right)^2\left(\mu_1-\mu_2\right)\left(\mu_1+\mu_2\right)}\cdot\\
&\quad\left(1+\frac{\lambda_1\mu_1\left(\lambda_1+2\mu_1\right)}{\left(\lambda_1+\mu_1\right)\left(\mu_1+\mu_2\right)\left(\mu_1-\mu_2\right)}\right.\\
&\quad\left.+\frac{\mu_1^2}{\left(\lambda_1+\mu_1\right)\left(\mu_1-\mu_2\right)}+\frac{\lambda_1}{\mu_1+\mu_2}\right). \qquad (61)
\end{aligned}$$

When $\Theta_{i-1}^{\zeta}=B$ and $\zeta=2$, we have

$$\begin{aligned}
&E\left[X_i^1Y_i^2 \mid \Theta_{i-1}^2=(B)\right]\\
&=E\left[X_i^1T_i^2\right]+E\left[X_i^1w_i^2\big|_{X_i^2<T_{i-1}^2+w_i^2}\right]\\
&=E\left[X_i^1\right]E\left[T_i^2\right]+E\left[X_i^1w_i^2\left(e^{-\mu_2X_i^2}+\mu_2X_i^2e^{-\mu_2X_i^2}\right)\right]\\
&=\frac{P_2^2}{1+P_2^2-P_4^2}\cdot\frac{\lambda_1^2\mu_1^3}{\left(\lambda_1+\mu_1\right)\left(\lambda_1+\mu_2\right)^2\left(\mu_1-\mu_2\right)\left(\mu_1+\mu_2\right)}\\
&\left(\frac{2}{\lambda_1+\mu_2}-\frac{2\mu_2}{\mu_1^2-\mu_2^2}+\frac{2\lambda_1\mu_1\left(\lambda_1+2\mu_1\right)}{\left(\lambda_1+\mu_1\right)\left(\mu_1+\mu_2\right)\left(\mu_1-\mu_2\right)}\right.\\
&\quad\cdot\left(\frac{1}{\lambda_1+\mu_2}-\frac{2\mu_2}{\mu_1^2-\mu_2^2}\right)+\frac{\mu_1^2}{\left(\lambda_1+\mu_1\right)\left(\mu_1-\mu_2\right)}\\
&\quad\cdot\left(\frac{2}{\lambda_1+\mu_2}-\frac{\mu_1+3\mu_2}{\mu_1^2-\mu_2^2}\right)\\
&\quad\left.+\frac{\lambda_1}{\mu_1+\mu_2}\cdot\left(\frac{2}{\lambda_1+\mu_2}+\frac{\mu_1-3\mu_2}{\mu_1^2-\mu_2^2}\right)\right). \qquad (62)
\end{aligned}$$

Similarly, we analyze $E[Y_i^{\zeta} \mid \Theta_{i-1}^{\zeta}=(Id/B)]$ in the first-hop. When $\Theta_{i-1}^{\zeta}=Id$ and $\zeta=1$, if $X_i^1>T_{i-1}^1$ then $Y_i^1=T_i^1$ and if $X_i^1<T_{i-1}^1$ then $Y_i^1=T_i^1+w_i^1$. We have

$$\begin{aligned}
E\left[Y_i^1 \mid \Theta_{i-1}^1=(Id)\right]&=E\left[T_i^1\right]+E\left[w_i^1\big|_{X_i^1<T_{i-1}^1}\right]\\
&=E\left[T_i^1\right]+E\left[w_i^1e^{-\mu_1X_i^1}\right]\\
&=\frac{1}{\mu_1}+\frac{1}{\mu_1\left(\lambda_1+\mu_1\right)}. \qquad (63)
\end{aligned}$$

When $\Theta_{i-1}^{\zeta}=B$ and $\zeta=1$, we have

$$\begin{aligned}
&E\left[Y_i^1 \mid \Theta_{i-1}^1=(B)\right]\\
&=E\left[T_i^1\right]+E\left[w_i^1\big|_{X_i^1<T_{i-1}^1+w_i^1}\right]\\
&=E\left[T_i^1\right]+E\left[w_i^1\left(e^{-\mu_1X_i^1}+\mu_1X_i^1e^{-\mu_1X_i^1}\right)\right]\\
&=\frac{1}{\mu_1}+\frac{1}{\mu_1\left(\lambda_1+\mu_1\right)}+\frac{\lambda_1}{\left(\lambda_1+\mu_1\right)^2}. \qquad (64)
\end{aligned}$$

Then, when it comes to the second-hop ($\zeta=2$), we have

$$\begin{aligned}
E\left[Y_i^2 \mid K_{i-1}^2=(B)\right]&=E\left[T_2^i\right]+E\left[w_i^2\big|_{X_i^2<T_2^{i-1}+w_{i-1}^2}\right]\\
&=E\left[T_2^i\right]+E\left[w_i^2\right]\left(E\left[e^{-\mu_2X_i^2}\right]+E\left[\mu_2X_i^2e^{-\mu_2X_i^2}\right]\right)\\
&=\frac{1}{\mu_2}+\frac{1}{\mu_2}P_4^2, \qquad (65)
\end{aligned}$$

and

$$\begin{aligned}
E\left[Y_i^2 \mid K_{i-1}^2=(Id)\right]&=E\left[T_2^i\right]+E\left[w_i^2e^{-\mu_2X_i^2}\right]\\
&=\frac{1}{\mu_2}+\frac{1}{\mu_2}P_2^2. \qquad (66)
\end{aligned}$$

For the analysis of PAoI, we first evaluate $E[(2X_i+Y_i)\|_{i=i^*} \mid K_{i-1}(Id)]$. In the first-hop, if $\Theta_{i-1}^1=(Id)$ and $X_i^1>T_{i-1}^1$, then $Y_i^1=T_1^i$; if $\Theta_{i-1}^1=(Id)$ and $X_i^1<T_{i-1}^1$, then $Y_i^1=T_1^i+w_i^1$. Due to the fact that the state of file $i-1$ is Id, we have $\Pr_1(i=i^* \mid \Theta_{i-1}^1=(Id))=1$. Therefore, we have

$$\begin{aligned}
&E\left[\left(2X_i^1+Y_i^1\right)\|_{i=i}^* \mid \Theta_{i-1}^1(Id)\right]\\
&=E\left[2X_i^1+T_1^i\right]+E\left[w_i^1\big|_{X_i^1<T_1^{i-1}}\right]\\
&=\frac{2}{\lambda_1}+\frac{1}{\mu_1}+\frac{\lambda_1}{\mu_1\left(\lambda_1+\mu_1\right)}. \qquad (67)
\end{aligned}$$

In the second-hop, if $\Theta_{i-1}^2=(Id)$ and $X_i^2>T_2^{i-1}$ ($X_i^2=X_i^1+Y_i^1-Y_{i-1}^1$), then $Y_i^2=T_2^i$; if $\Theta_{i-1}^2=(Id)$ and $X_i^2<T_2^{i-1}$, then $Y_i^2=T_2^i+w_i^2$. Similarly, with $\Pr_2(i=i^* \mid \Theta_{i-1}^2=(Id))=1$, we have

$$\begin{aligned}
&E\left[Y_i^2\|_{i=i^*} \mid \Theta_{i-1}^2(Id)\right]\\
&=E\left(T_2^i\right)+E\left[w_i^2\big|_{X_i^2T_2^{i-1}}\right]=\frac{1}{\mu_2}+\frac{1}{\mu_2}P_2^2. \qquad (68)
\end{aligned}$$

Next, we evaluate $E[(2X_i+Y_i)\|_{i=i^*} \mid \Theta_{i-1}(B)]$. When it is in the B state ($\Theta_{i-1}^1=(B)$) in the first-hop, if $X_i^1>T_1^{i-1}+w_{i-1}^1$, then $Y_i^1=T_1^i$; else ($w_{i-1}^1<X_i^1<T_1^{i-1}+w_{i-1}^1$), $Y_i^1=T_1^i+w_i^1$. Moreover, if the interval time $X_i^1<w_{i-1}^1$, then the indicator function satisfies $\|_{i=i^*}=0$, and we have $\Pr(i=i^* \mid \Theta_{i-1}^1=(B))=1-\frac{\lambda_1}{\lambda_1+\mu_1}$. Therefore, we get

$$\begin{aligned}
&E\left[\left(2X_i^1+Y_i^1\right)\|_{i=i^*} \mid \Theta_{i-1}^1(B)\right]\\
&=E\left[\left(2X_i^1+T_1^i\right)\left(1-e^{-\mu_1X_i^1}\right)\right]+E\left[w_i^1\mu_1X_i^1e^{-\mu_1X_i^1}\right]
\end{aligned}$$

$$= \frac{2}{\lambda_1} + \frac{1}{\mu_1} - \frac{\lambda_1}{\mu_1(\lambda_1+\mu_1)} - \frac{\lambda_1}{(\lambda_1+\mu_1)^2}. \quad (69)$$

When it is in the B state ($\Theta_{i-1}^1 = (B)$) in the second-hop, if $X_i^2 > T_2^{i-1} + w_{i-1}^2$ ($X_i^2 = X_i^1 + Y_i^1 - Y_{i-1}^1$), then $Y_i^2 = T_2^i$; else ($w_{i-1}^2 < X_i^2 < T_2^{i-1} + w_{i-1}^2$), $Y_i^2 = T_2^i + w_i^2$. Therefore, we have

$$\begin{aligned} &E\left[Y_i^2\|_{i=i^*} \mid \Theta_{i-1}^2(B)\right] \\ &= E\left[T_2^i\left(1-e^{-\mu_2 X_i^2}\right)\right] + E\left[w_i^2\mu_2 X_i^2 e^{-\mu_2 X_i^2}\right] \\ &= \frac{1}{\mu_2} - \frac{1}{\mu_2}\left(2P_2^2 - P_4^2\right). \end{aligned} \quad (70)$$

Therefore, we can get the average AoI (18) and PAoI (22) through the above derivation.

REFERENCES

[1] J. Jiao et al., "Network utility maximization resource allocation for NOMA in satellite-based Internet of Things," *IEEE Internet Things J.*, vol. 7, no. 4, pp. 3230–3232, Apr. 2020.

[2] L. Bai et al., "A novel atmosphere-informed data-driven predictive channel modeling for B5G/6G satellite-terrestrial wireless communication systems at Q-band," *IEEE Trans. Veh. Technol.*, vol. 69, no. 12, pp. 14225–14237, Dec. 2020.

[3] R. Sturdivantt et al., "System latency performance of mechanical and electronic scanned antennas for LEO ground stations for IoT and internet access," in *Proc. Topical Workshop Internet Space*, 2017, pp. 1–4.

[4] Y. Shi, J. Liu, Z. M. Fadlullah, and N. Kato, "Cross-layer data delivery in satellite-aerial-terrestrial communication," *IEEE Wireless Commun.*, vol. 25, no. 3, pp. 138–143, Jun. 2018.

[5] J. Liu, Y. Shi, Z. M. Fadlullah, and N. Kato, "Space-air-ground integrated network: A survey," *IEEE Commun. Surv. Tuts.*, vol. 20, no. 4, pp. 2714–2741, Oct.–Dec. 2018.

[6] D. Li et al., "Age-optimal HARQ design for freshness-critical satellite-IoT systems," *IEEE Internet Things J.*, vol. 7, no. 3, pp. 2066–2076, Mar. 2020.

[7] S. Kaul, M. Gruteser, V. Rai, and J. Kenney, "Minimizing age of information in vehicular networks," in *Proc. IEEE 8th Annu. Commun. Soc. Conf. Sensor, Mesh Ad Hoc Commun. Netw.*, 2011, pp. 350–358.

[8] Y. Sun et al., "Update or wait: How to keep your data fresh," in *Proc. IEEE 5th Annu. Int. Conf. Comput. Commun.*, 2016, pp. 1–9.

[9] L. Shi et al., "Integration of reed-solomon codes to licklider transmission protocol (LTP) for space DTN," *IEEE Aerosp. Electron. Syst. Mag.*, vol. 32, no. 4, pp. 48–55, Apr. 2017.

[10] CCSDS 131.5-O-1, Erasure correcting codes for use in near-earth and deep-space communications, 2014. [Online]: https://public.ccsds.org/Pubs/131x5o1.pdf

[11] S. Liu et al., "Age-optimal NC-HARQ protocol for multi-hop satellite-based Internet of Things," in *Proc. IEEE Wireless Commun. Netw. Conf.*, Nanjing, China, 2021, pp. 1–6.

[12] S. Kaul et al., "Real-time status: How often should one update?," in *Proc. IEEE INFOCOM*, 2012, pp. 2731–2735.

[13] P. Zou et al., "On the benefits of waiting in status update systems," in *Proc. IEEE Conf. Comput. Commun. Workshops*, 2019, pp. 171–176.

[14] P. Zou et al., "Trading off computation with transmission in status update systems," in *Proc. IEEE 30th Annu. Int. Symp. Pers.*, 2019, pp. 1–6.

[15] X. Cao, F. Wang, J. Xu, R. Zhang, and S. Cui, "Joint computation and communication cooperation for energy-efficient mobile edge computing," *IEEE Internet Things J.*, vol. 6, pp. 4188–4200, Jun. 2019.

[16] Q. Kuang et al., "Age-of-information for computation-intensive messages in mobile edge computing," in *Proc. IEEE Int. Conf. Wireless Commun. Signal Process.*, 2019, pp. 1–6.

[17] B. Soret et al., "Latency and timeliness in multi-hop satellite networks," in *Proc. IEEE Int. Conf. Commun.*, 2020, pp. 1–6.

[18] C. J. Le Martret et al., "Analytical performance derivation of hybrid ARQ schemes at IP layer," *IEEE Trans. Commun.*, vol. 60, no. 5, pp. 1305–1314, May 2012.

[19] E. Khorov, A. Krasilov, and A. Malyshev, "Radio resource and traffic management for ultra-reliable low latency communications," in *Proc. IEEE Wireless Commun. Netw. Conf.*, pp. 1–6, 2018.

[20] P. Wu and N. Jindal, "Coding versus ARQ in fading channels: How reliable should the PHY be?," *IEEE Trans. Commun.*, vol. 59, no. 12, pp. 3363–3374, Dec. 2011.

[21] W. Lee, O. Simeone, J. Kang, S. Rangan, and P. Popovski, "HARQ buffer management: An information-theoretic view," *IEEE Trans. Commun.*, vol. 63, no. 11, pp. 4539–4550, Nov. 2015.

[22] G. Caire and D. Tuninetti, "The throughput of hybrid-ARQ protocols for the Gaussian collision channel," *IEEE Trans. Inf. Theory*, vol. 47, no. 5, pp. 1971–1988, Jul. 2001.

[23] B. Makki and T. Eriksson, "On hybrid ARQ and quantized CSI feedback schemes in quasi-static fading channels," *IEEE Trans. Commun.*, vol. 60, no. 4, pp. 986–997, Apr. 2012.

[24] B. Makki, T. Svensson, G. Caire, and M. Zorzi, "Fast HARQ over finite blocklength codes: A technique for low-latency reliable communication," *IEEE Trans. Wireless Commun.*, vol. 18, no. 1, pp. 194–209, Jan. 2019.

[25] M. Shirvanimoghaddam, H. Khayami, Y. Li, and B. Vucetic, "Dynamic HARQ with guaranteed delay," in *Proc. IEEE Wireless Commun. Netw. Conf.*, 2020, pp. 1–6.

[26] CCSDS 734.1-B-1, Licklider transmission protocol (LTP) for CCSDS [2015], [Online]: https://public.ccsds.org/Pubs/734x1b1.pdf

[27] A. Javani, M. Zorgui, and Z. Wang, "On the age of information in erasure channels with feedback," in *Proc. IEEE Int. Conf. Commun.*, 2020, pp. 1–6.

[28] Y. Wang, S. Wu, J. Jiao, W. Wu, Y. Wang, and Q. Zhang, "Age-optimal transmission policy with HARQ for freshness-critical vehicular status updates in space-air-ground integrated networks," *IEEE Internet Things J.*, vol. 9, no. 8, pp. 5719–5729, Apr. 2022.

[29] J. Jiao, Y. He, Y. Wang, and S. Wu, "Design and analysis of novel Ka band NOMA uplink relay system for Lunar farside exploration," *China Commun.*, vol. 17, no. 7, pp. 1–14, Jul. 2020.

[30] A. Abdi, W. C. Lau, M. Alouini, and M. Kaveh, "A new simple model for land mobile satellite channels: First-and second-order statistics," *IEEE Trans. Wireless Commun.*, vol. 2, no. 3, pp. 519–528, May 2003.

[31] M. R. Bhatnagar and A. M. K., "On the closed-form performance analysis of maximal ratio combining in Shadowed-Rician fading LMS channels," *IEEE Commun. Lett.*, vol. 18, no. 1, pp. 54–57, Jan. 2014.

[32] J. Jiao, X. Sui, S. Gu, S. Wu, and Q. Zhang, "Partially observable Markov decision process-based transmission policy over Ka-band channels for space information networks," *Entropy*, vol. 19, no. 10, 2017, Art. no. 510.

[33] S. V. Amari and R. B. Misra, "Closed-form expressions for distribution of sum of exponential random variables," *IEEE Trans. Rel.*, vol. 46, no. 4, pp. 519–522, Dec. 1997.

[34] ETSI EN 302 307, Digital video broadcasting (DVB); second generation framing structure, channel coding and modulation systems for broadcasting, interactive services, news gathering and other broadband satellite applications (DVB-S2) [2009], [Online]: http://www.etsi.org/deliver/etsi_en/302300_302399/302307/01.02.01_60 /en_302307v010201p.pdf

[35] A. M. K. and S. K. Jindal, "OSTBC transmission in shadowed-rician land mobile satellite links," *IEEE Trans. Veh. Technol.*, vol. 65, no. 7, pp. 5771–5777, Jul. 2016.

Jian Jiao (Member, IEEE) received the M.S. and Ph.D. degrees in communication engineering from the Harbin Institute of Technology (HIT), in 2007 and 2011, respectively. From 2011 to 2015, he was a Postdoctoral Research Fellow of Communication Engineering Research Centre, Shenzhen Graduate School, HIT, Shenzhen, China. From 2016 to 2017, he was a China Scholarship Council Visiting Scholar with the School of Electrical and Information Engineering, The University of Sydney, Sydney, NSW, Australia. From 2017 to 2019, he was an Assistant Professor with the Harbin Institute of Technology (Shenzhen) (HITsz), Shenzhen, China, where he has been an Associate Professor with the Department of Electrical and Information Engineering since 2020. He is also an Associate Professor with Peng Cheng Laboratory, Shenzhen, China. His current research interests include error control codes, satellite communications and networking, and massive random access.

Shiqi Liu received the bachelor's degree in communication engineering from Harbin Engineering University, Harbin, China, in 2019, and the master's degree in electronics and communication engineering from the Harbin Institute of Technology (Shenzhen), Shenzhen, China, in 2022. His research interests include satellite communications and age of information.

Jing Ding received the B.S. degree in communication engineering from Zhengzhou University, Zhengzhou, China, in 2020. He is currently working toward the graduation degree with the Harbin Institute of Technology (Shenzhen), Shenzhen, China. His current research interests include satellite-based Internet of Things, HARQ, and age of information.

Jianhao Huang received the B.S. degree in communication engineering from the Harbin Institute of Technology (Shenzhen), China, in 2022. He is currently working toward the M.S. degree with the Harbin Institute of Technology (Shenzhen), Shenzhen, China. His current research interests include satellite communications and age of information.

Shaohua Wu (Member, IEEE) received the Ph.D. degree in communication engineering from the Harbin Institute of Technology, Harbin, China, in 2009. From 2009 to 2011, he was a Postdoctoral with the Department of Electronics and Information Engineering, Shenzhen Graduate School, Harbin Institute of Technology (Shenzhen), Shenzhen, China, where he was an Associate Professor from 2012 to 2020. Since 2021, he has been a Professor with the School of Electrical and Information Engineering, Harbin Institute of Technology (Shenzhen), and also a Professor with Peng Cheng Laboratory, Shenzhen, China. His current research interests include wireless image/video transmission, space communications, advanced channel coding techniques, and B5G wireless transmission technologies.

Rongxing Lu (Fellow, IEEE) received the Ph.D. degree from the Department of Electrical and Computer Engineering, University of Waterloo, Waterloo, ON, Canada, in 2012. He is currently a Mastercard IoT Research Chair, University Research Scholar, an Associate Professor with the Faculty of Computer Science (FCS), University of New Brunswick (UNB), Fredericton, NB, Canada. Before that, he was an Assistant Professor with the School of Electrical and Electronic Engineering, Nanyang Technological University (NTU), Singapore, from April 2013 to August 2016. From May 2012 to April 2013, he was a Postdoctoral Fellow with the University of Waterloo, Waterloo, ON, Canada. He has authored or coauthored extensively in his areas of expertise. His research interests include applied cryptography, privacy enhancing technologies, and IoT-Big Data security and privacy. He was awarded the most prestigious Governor General's Gold Medal, when he received the Ph.D. degree. He won the 8th IEEE Communications Society (ComSoc) Asia Pacific (AP) Outstanding Young Researcher Award, in 2013. He was the recipient of nine best (student) paper awards from some reputable journals and conferences and the winner of 2016-2017 Excellence in Teaching Award from FCS, UNB. He is the Chair of IEEE ComSoc Communications and Information Security Technical Committee (CIS-TC), and the founding Co-Chair of IEEE TEMS Blockchain and Distributed Ledgers Technologies Technical Committee (BDLT-TC).

Qinyu Zhang (Senior Member, IEEE) received the bachelor's degree in communication engineering from the Harbin Institute of Technology (HIT), Harbin, China, in 1994, and the Ph.D. degree in biomedical and electrical engineering from the University of Tokushima, Tokushima, Japan, in 2003. From 1999 to 2003, he was an Assistant Professor with the University of Tokushima. Since 2003, he has been with the Harbin Institute of Technology (Shenzhen) (HITsz), Shenzhen, China, where he is currently a Full Professor and the Dean of the EIE School. His research interests include aerospace communications and networks, and wireless communications and networks. He has been awarded the National Science Fund for Distinguished Young Scholars, Young and Middle-Aged Leading Scientist of China, and Chinese New Century Excellent Talents in University, and was the recipient of three scientific and technological awards from governments.